YGS Open File 2017-3

Curie point depth mapping in Yukon

Jeff Witter, *Innovate Geothermal Ltd*
and Craig Miller, *Simon Fraser University*

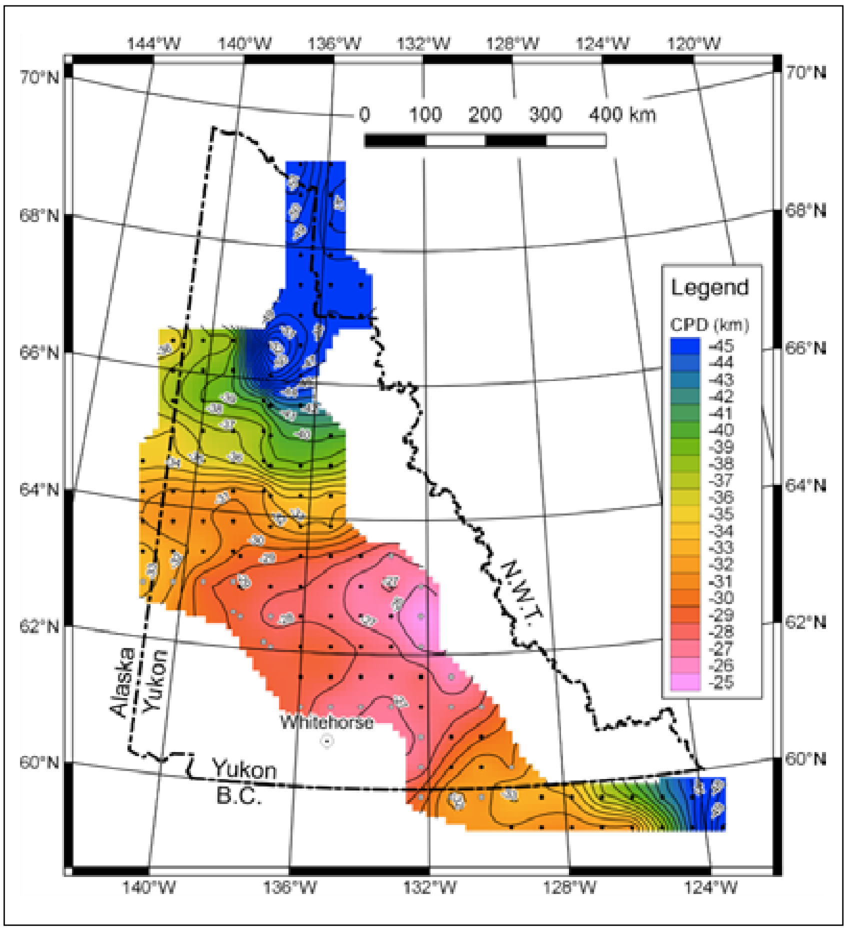

Yukon Geological Survey • Innovate Geothermal • SFU Simon Fraser University • Yukon Energy, Mines and Resources

Published under the authority of the Department of Energy, Mines and Resources, Government of Yukon http://www.emr.gov.yk.ca.

Printed in Whitehorse, Yukon, 2017.

Publié avec l'autorisation du Ministères de l'Énergie, des Mines et des Ressources du gouvernement du Yukon, http://www.emr.gov.yk.ca.

Imprimé à Whitehorse (Yukon) en 2017.

This, and other Yukon Geological Survey publications, may be obtained from:

Yukon Geological Survey

102-300 Main Street

Box 2703 (K-102)

Whitehorse, Yukon, Canada Y1A 2C6

phone (867) 667-3201, e-mail geology@gov.yk.ca

Visit the Yukon Geological Survey website at www.geology.gov.yk.ca.

In referring to this publication, please use the following citation:

Witter, J. and Miller, C., 2017. Curie point depth mapping in Yukon. Yukon Geological Survey, Open File 2017-3, 37 p.

EXECUTIVE SUMMARY

We performed Curie point depth (CPD) mapping in Yukon using public domain aeromagnetic data from Natural Resources Canada. CPD mapping estimates the depth in the Earth's crust to the Curie point temperature (~580°C) where magnetization in rocks disappears. When used in combination with other data, such as heat flow, CPD mapping can serve as a regional scale geothermal prospecting tool. In this study, two different CPD methodologies were employed using two different window sizes (200 km and 300 km). Qualitatively, the results were broadly consistent regardless of the method or window size. South-central Yukon exhibits shallow CPD values while northern and southeastern Yukon have deeper CPD values. This suggests that south-central Yukon has higher levels of heat flow in the mid-to-lower crust compared to the rest of the territory. The CPD results are largely consistent with heat flow measurements from the near surface. Specifically, regions with shallow CPD estimates correspond to areas with elevated heat flow measurements. Geologically, the regions with shallow CPD correspond to the Cordillera, while deep CPD areas appear to be co-located with continental platform rocks of Ancestral North America. Comparison with Yukon-specific crustal geotherms derived from other data suggest that the CPD estimates for south-central Yukon are systematically too deep by 2 to 12 km. The discrepancy is likely caused by the need to better understand and account for the fractal distribution of magnetization in the crust in Yukon. The results of this CPD study are valuable in that 95% of Yukon has been demarcated into regions of shallow CPD (higher heat flow) and deep CPD (lower heat flow). These findings should be combined with other data, such as heat generation and sediment thickness estimates, to identify the most prospective regions of elevated subsurface heat in Yukon.

CONTENTS

LIST OF FIGURES

INTRODUCTION

This report presents the results of a Curie point depth (CPD) mapping study across the entire Yukon. CPD mapping is a methodology, originally developed in the 1970s, which utilizes regional-scale aeromagnetic survey data to map the depth in the Earth's crust to the Curie point temperature (~580°C) where magnetization in rocks disappears. CPD mapping has been used in combination with other methods (such as heat flow measurements) in many parts of the world as a regional scale geothermal prospecting tool. One advantage of CPD mapping is it can provide information on crustal temperatures at depths not accessible by other means (Okubo *et al.*, 1985). Examples of previous CPD studies include regional or country-wide compilations in the USA, Indonesia, Japan, Turkey, Mexico, Afghanistan, Venezuela, Egypt, South Africa, Germany and Taiwan (Arnaiz-Rodriguez and Orihuela, 2013; Aydin *et al.*, 2005; Bansal *et al.*, 2011; Bilim *et al.*, 2016; Bouligand *et al.*, 2009; Espinosa-Cardeña and Campos-Enriquez, 2008; Hseih *et al.*, 2014; Manea and Manea, 2011; Nyabeze and Gwavava, 2016; Okubo *et al.*, 1985; Okubo *et al.*, 1989; Saada, 2016; Saibi *et al.*, 2015; Tanaka *et al.*, 1999). Regions found to have shallow Curie point depths are expected to have higher heat flow, higher average temperature gradient, and, therefore, a higher likelihood of geothermal energy resources that are accessible via drilling. The CPD mapping method is particularly suited for Yukon because of the availability of public domain magnetic survey data that cover most the territory (Fig. 1). Heat flow data for Yukon are limited in extent (Fig. 2), thus, due to the broad, regional nature of the CPD technique, the results of this study can complement existing data to help better understand heat flow variations across the territory. The results of the CPD analysis described here are compared with other indicators of geothermal resources such as high heat flow, known volcanism, and hot springs. In addition, the CPD maps generated in this study are interpreted in the context of regional, crustal-scale geology as well as other studies of crustal geotherms in Yukon.

DATA

The magnetic data used in this study were obtained from the Natural Resources Canada Geoscience Data Repository for Geophysical Data (http://gdr.agg.nrcan.gc.ca/), accessed in January 2017. These data are residual total field magnetic data that have been compiled from multiple airborne magnetic surveys collected over many years at different survey heights using both fixed-wing and helicopter platforms. The data are levelled by NRCAN to a common altitude of 100 m above the terrain. The primary magnetic dataset used for this study covers ~95% of Yukon and has a spatial resolution of 200 m. No magnetic data are available for the southwestern corner of the territory in the St. Elias mountain range (Fig. 1). The Yukon-wide magnetic data are supplemented by two additional datasets: 100 m resolution magnetic data in a wide corridor along the Alaska-Yukon border and 200 m resolution magnetic data extending into British Columbia and Northwest Territories (Fig. 1). The purpose of the supplementary magnetic data is to extend the CPD analysis along the southern, northern, and western borders of Yukon. Overall, the magnetic data analyzed in this study cover an area of >500 000 km^2.

The heat flow map shown in Figure 2 was extracted from a Canada-wide heat flow compilation published in Grasby *et al.* (2012). The heat flow values are based upon high quality downhole temperature logs as well as variable quality point measurements (*e.g.*, bottom hole temperatures and drill stem tests). Individual heat flow data points for central and southern Yukon were derived from Lewis *et al.* (2003).

Locations of Holocene volcanoes in Yukon were obtained from the Smithsonian Institution Global Volcanism Program (http://volcano.si.edu/). Holocene volcanoes are those which have erupted in the last ~10 000 years. Additional information on past volcanism in Yukon was obtained from Edwards and Russell (2000) which lists the locations of Neogene-to-Quaternary volcanic centres (*i.e.*, younger than ~23 million years).

Locations of hot springs in Yukon were obtained from the Yukon Geological Survey. Discharge temperatures of the hot springs within the territory range up to 47°C measured at Takhini Hot Springs which is located ~28 km northwest of Whitehorse.

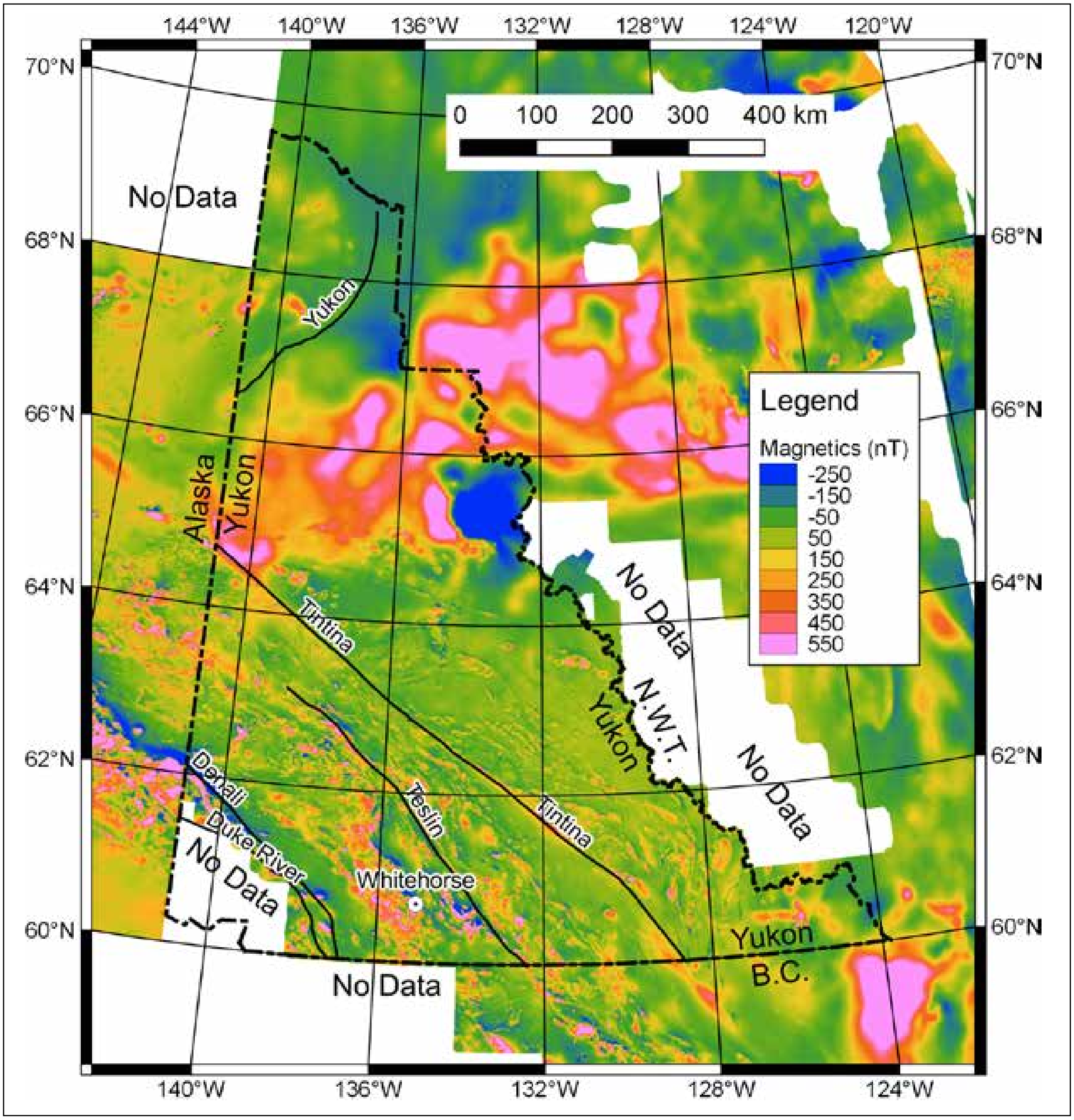

Figure 1. *Map showing the distribution of public domain, magnetic data for Yukon as Residual Total Field in units of nanoTesla (nT). Warm colours represent magnetic highs and cool colours, magnetic lows. White areas have no magnetic data. Black lines depict major faults (Colpron and Nelson, 2011). Map is in Yukon Albers NAD83.*

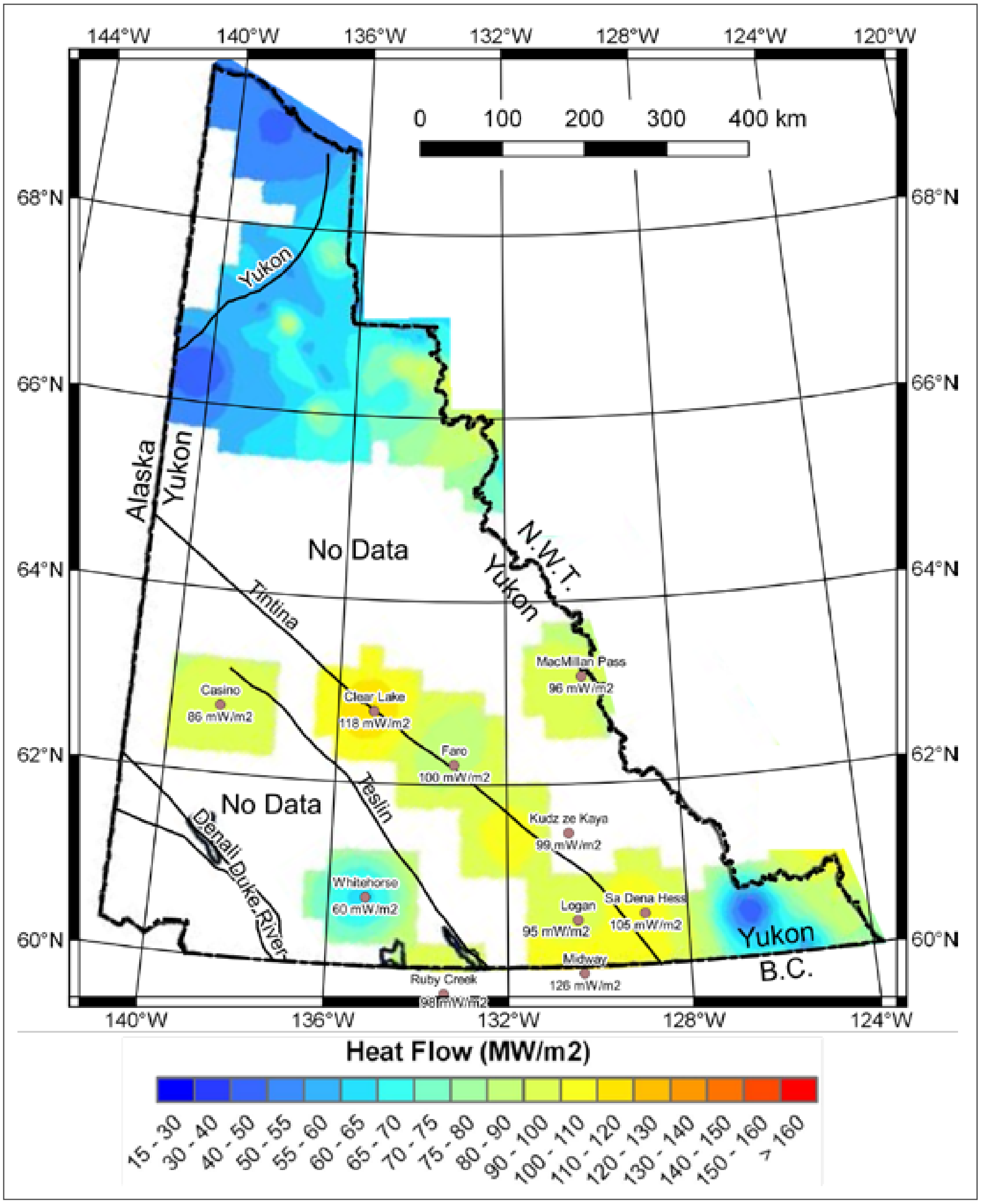

Figure 2. *Heat flow map of Yukon from Grasby et al. (2012). Warm colours represent high heat flow and cool colours, low heat flow. Selected heat flow data points from Lewis et al. (2003) are also shown as brown dots labelled with the location and heat flow value. Portions of central and southern Yukon show elevated heat flow compared to other parts of Yukon. Much of the territory lacks heat flow measurements. Black lines depict major faults (Colpron and Nelson, 2011). Map is in Yukon Albers NAD83.*

METHODOLOGY

The idea of using magnetic data to estimate the depth to the Curie point arose in the mid-20th century (Vacquier and Affleck, 1941). But it wasn't until the topic was revisited in the 1970-80s that a workable methodology was developed (Spector and Grant, 1970; Bhattacharyya and Leu, 1975; Shuey *et al.*, 1977; Connard *et al.*, 1983; Okubo *et al.*, 1985; Blakely, 1988; Okubo *et al.*, 1989). Further refinements to the method in the 1990s (*e.g.*, Tanaka *et al.*, 1999) resulted in one of two CPD mapping techniques that we employ in this study.

The Tanaka *et al.*, (1999) CPD mapping method assumes that long wavelength magnetic anomalies are related to large-sized magnetic sources that have a random and uncorrelated distribution within the Earth's crust. These magnetic sources extend to depths of a few to tens of kilometres. The bottoms of these magnetic sources are assumed to correspond to the ~580°C Curie Point temperature. Each CPD estimate is calculated at the centre of a square magnetic data "window" that has dimensions large enough to contain the long wavelength information required to derive the CPD value at any given location. Calculation windows are commonly overlapped with adjacent windows to increase the density of CPD estimates and to enhance the spatial continuity of the generated CPD map. If a window contains a portion of no data then the calculation is not possible which results in a gap in the coverage. The depth to the bottom of the magnetic source (*i.e.*, assumed to correspond to the Curie point depth) is calculated in this study in four steps using the Tanaka *et al.*, (1999) method:

1. calculate the radially averaged power spectrum of the magnetic data in each window;
2. estimate the depth to the top of the magnetic source (Z_t) using the high wave number portion of the magnetic anomaly power spectra;
3. estimate the depth to the centroid of the magnetic source (Z_o) using a lower wave number portion of the magnetic anomaly power spectra; and
4. calculate the depth to the bottom of the magnetic source (Z_b) using the following equation:

   $$Z_b = 2Z_o - Z_t \quad (1)$$

   The value of Z_b is assumed to be the CPD.

Other studies (*e.g.*, Pilkington and Todoeschuck, 1993; Maus *et al.*, 1997; Pilkington *et al.*, 2006; Bouligand *et al.*, 2009; Chopping and Kennett, 2015) point out that for some portions of the Earth's crust, the assumption of randomly distributed magnetic sources (*e.g.*, Tanaka *et al.*, 1999) is not applicable. Instead of a random distribution, magnetic sources may have a fractal distribution in the Earth's crust. Bansal *et al.* (2011) developed a method which extends the Tanaka *et al.* (1999) approach to incorporate an approximate correction factor to account for fractal distribution of magnetic sources. The fractal character of magnetic sources is captured in a fractal parameter β which may vary between ~1 and ~6 from place to place (Bouligand *et al.*, 2009). Unfortunately, the most appropriate value of β for Yukon is not well-defined. Yukon geology is dominated by the Canadian Cordillera, and Bouligand *et al.* (2009) estimated an average value of $\beta=3$ for the Cordillera of the western United States. Therefore, by analogy, a value of $\beta=3$ may be appropriate for Yukon. Regrettably, the Bansal *et al.* (2011) approximation method only works up to a maximum value of $\beta=2$ so we adopt this value for fractal CPD calculations in Yukon. The Bansal *et al.* (2011) method is similar to the Tanaka *et al.* (1999) approach in that the values of Z_t and Z_o are determined using graphs of power spectra, as described above. After we calculated CPD using the Tanaka *et al.* (1999) method, we also calculated CPD using Bansal *et al.* (2011) for comparison.

For this study, CPD values were calculated using two different window sizes: 200 km by 200 km square windows and 300 km by 300 km square windows. Various authors suggest that the window size should be ~6 to 10 times the depth to the CPD (Campos-Enriquez *et al.*, 1990; Ravat *et al.*, 2007). Windows were created in an overlapping manner such that window centres were offset from one another by 50 km in eastern and northern directions (Figs. 3 and 4).

Unfortunately, due to magnetic data gaps, it is not possible to completely cover Yukon with CPD data points. The large window sizes necessary for this study create ~100 to 150-km-wide buffers along the edge of no data zones. Window sizes smaller than 200 km are not viable because they would not capture the long wavelength signal required to estimate CPD in Yukon. Similarly, a 300 km window size effectively captures long wavelengths but provides less coverage. Magnetic data gaps are found in southwestern Yukon, northwestern British Columbia, westernmost Northwest Territories and northeastern Alaska (Fig. 1). No CPD estimates were possible in southeastern Yukon due to one of the data gaps. Therefore, we calculated CPD in the northeastern corner of British Columbia as a proxy for CPD in southeastern Yukon.

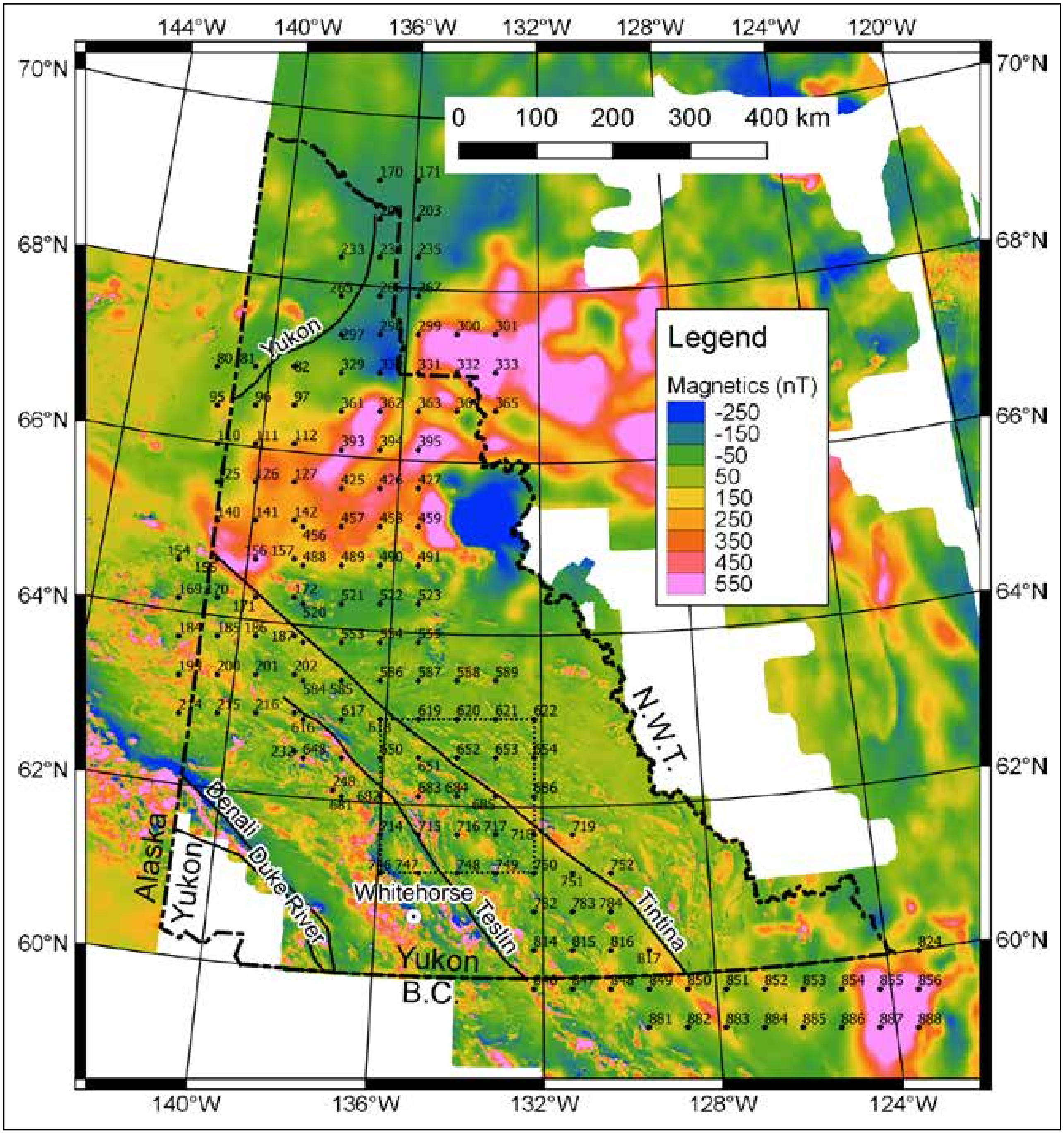

Figure 3. *Map showing the centre point locations of the 150 windows, each 200 km in size, used to calculate CPD. The numbers for the window centres are not consecutive. The dotted line outlines the 200 km x 200 km magnetic data window used to calculate CPD at location #684. The magnetic field data used in the study are shown in the background in units of nanoTesla. Black lines depict major faults (Colpron and Nelson, 2011). Map is in Yukon Albers NAD83.*

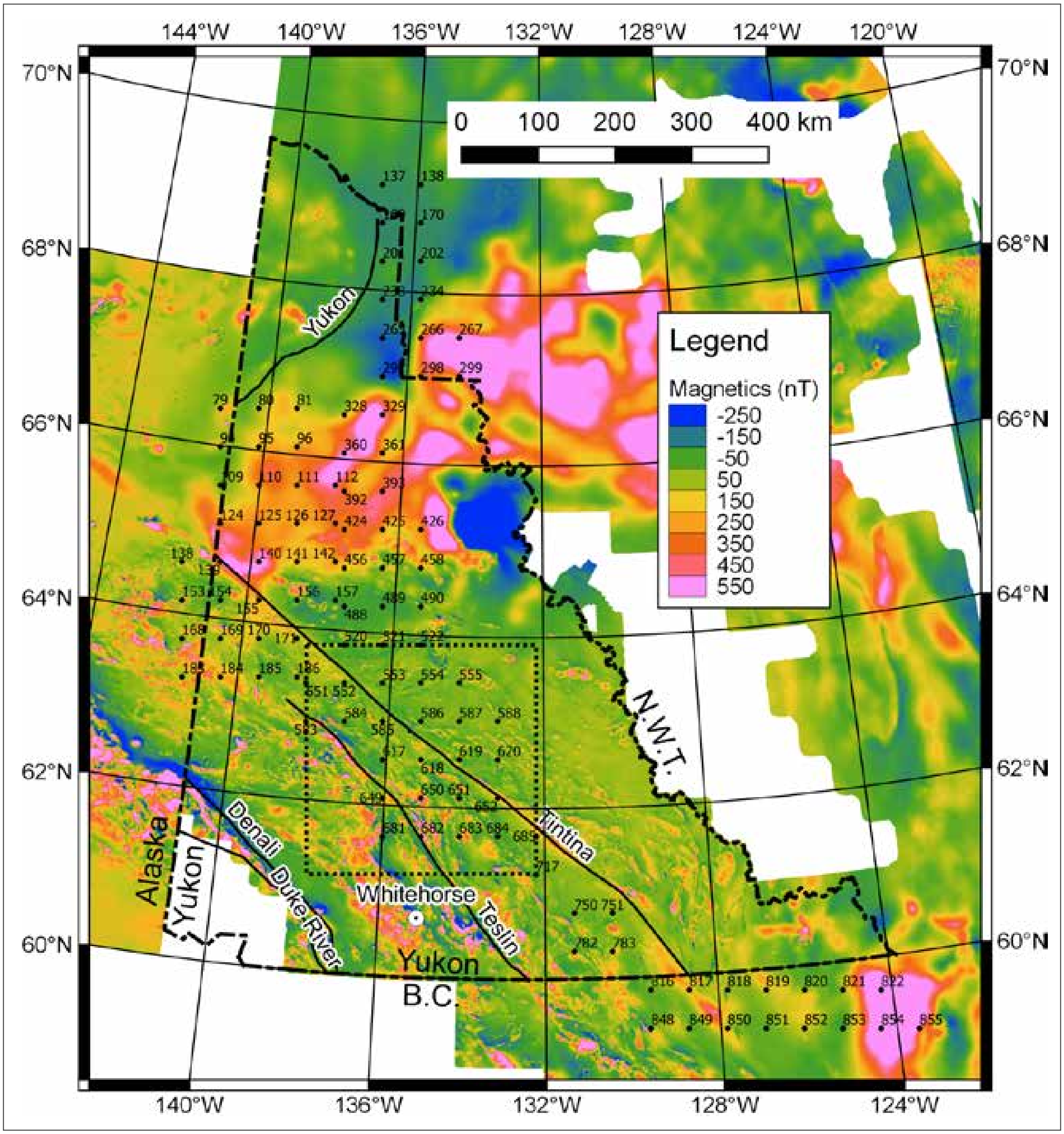

Figure 4. *Map showing the centre point locations of the 108 windows, each 300 km in size, used to calculate CPD. The numbers for the window centres are not consecutive. The dotted line outlines the 300 km x 300 km magnetic data window used to calculate CPD at location #618. The magnetic field data used in the study are shown in the background in units of nanoTesla. Black lines depict major faults (Colpron and Nelson, 2011). Map is in Yukon Albers NAD83.*

Here are some specifics of the CPD calculations using the Tanaka *et al.* (1999) method (random distribution of magnetic sources). For each window, the power spectrum was calculated using the grdfft function in the Generic Mapping Tools software (http://gmt.soest.hawaii.edu/) and then plotted vs. wavenumber according to Tanaka *et al.* (1999). The depth to top (Z_t) and depth to centroid (Z_o) of the magnetic source were calculated from slopes of lines in the power spectra graphs (*see* example in Fig. 5 and equations in Tanaka *et al.*, 1999).

In the scientific literature on CPD mapping, there is no specific and defined wavenumber range for calculating the slopes to determine Z_o and Z_t. We experimented with different high and low wavenumber ranges to calculate slopes for determining Z_o and Z_t in order to assess the sensitivity of our choices. We found that varying the selected wavenumber range by reasonable amounts changed the Z_o, Z_t and Z_b values by less than 10%. We used the same high and low wavenumber ranges for all windows to calculate the slopes for Z_t and Z_o. These wavenumber ranges are: 0.05-0.14 (Z_t) and 0.003-0.036 (Z_o).

For the CPD calculations using the Bansal *et al.* (2011) method (fractal distribution of magnetic sources), we employed the same approach used above to estimate CPD but also implemented Equations 7 and 8 in Bansal *et al.* (2011). Again, the selection of wavenumber ranges for calculating Z_o and Z_t is somewhat subjective, so for each spectrum, we visually identified the linear part of the curve and then assigned the appropriate wavenumber range. These linear segments were readily apparent and the selected wavenumber ranges fell into two groups for Z_t (0.025-0.05 and 0.05-0.1) and one group for Z_o (0.003-0.02).

Some limitations of the CPD mapping method include the following. First, long wavelength noise in the magnetic field may be present and can be challenging to detect, especially in a compilation of magnetic survey data such as the one used here. Such noise may cause the results of CPD calculations to be inaccurate (Blakely, 1988). Second, the magnetic source base depth (Z_b) may not represent the Curie point depth at all, but instead could simply be a geologic contact between magnetic and non-magnetic rocks. If this is the case, the calculated CPD may be unrelated to crustal temperatures and the Curie point temperature may actually lie at greater depths. Despite these limitations, a comparison of many CPD studies by Ravat *et al.* (2007) showed that most CPD estimates may be accurate to within a few kilometres. For a more detailed explanation of the methodology utilized in this study see Tanaka *et al.* (1999) and Bansal *et al.* (2011).

QUALITY CONTROL

Prior to generating maps that display CPD across Yukon, the results were reviewed for quality control. This effort had two parts:

1. visually review the magnetic data in each window; and
2. visually inspect and calculate the fit between the Z_o and Z_t lines (used to calculate CPD) and the power spectra, to ensure the fit ranges are appropriate.

The magnetic data used in this study consist of many surveys stitched together and levelled to a common survey elevation. One concern is that magnetic survey data collected in different parts of Yukon at different times using different airborne survey parameters could result in systematic differences in the power spectra from one window to the next. Such differences could potentially result in inaccurate CPD estimates. We reviewed the magnetic data in each window and identified survey artifacts in some areas (*e.g.*, "striping" of the magnetic data, "suture" lines where two separate magnetic survey datasets appear to have been stitched together, and adjacent magnetic regions with clear differences in frequency content related to differing flight altitudes). We found no correlation between the visual features observed in the magnetic data windows and low quality spectra. We conclude that the visual artifacts may be too high frequency to affect the long wavelength information in the magnetic data used to calculate CPD. It is unknown if data artifacts are present in the long wavelength portion of the magnetic data compilation.

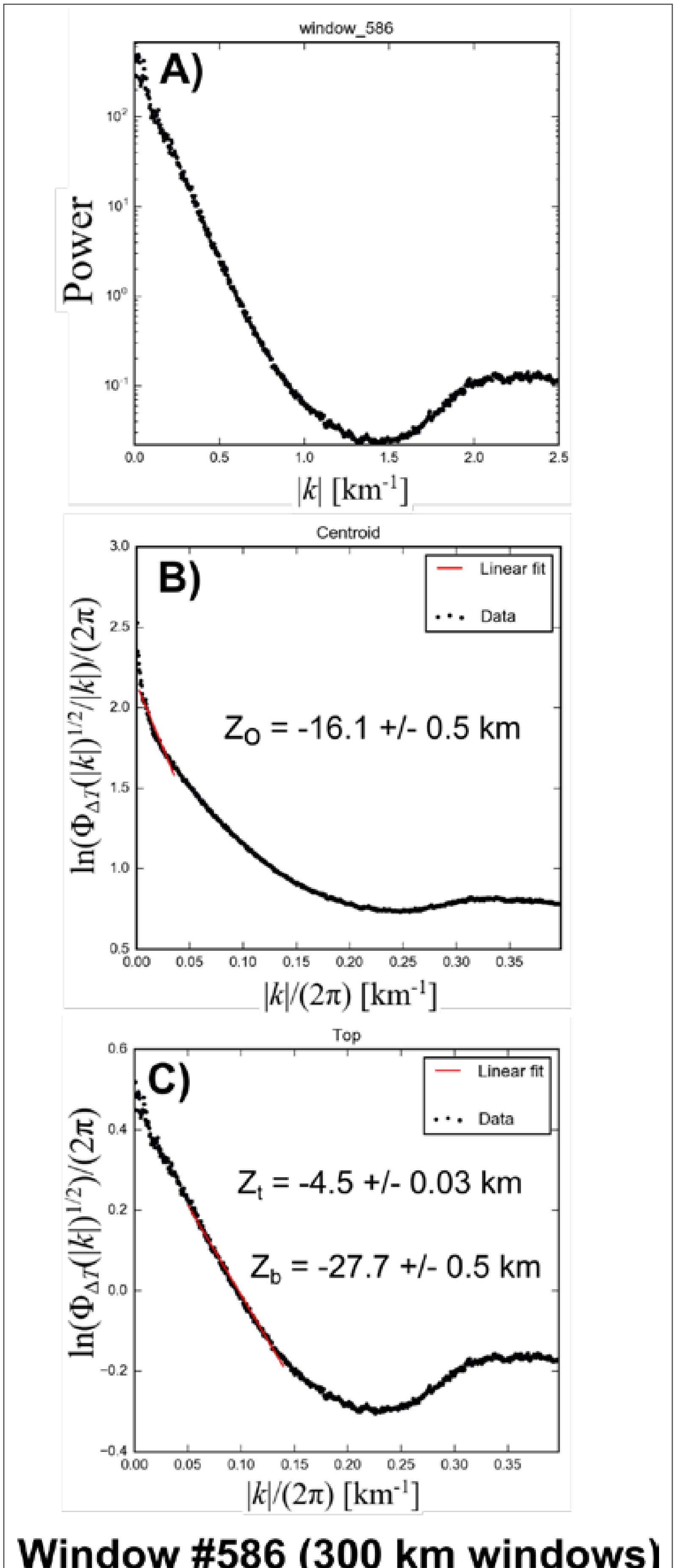

Figure 5. *A) Plot of magnetic power spectrum vs. wavenumber for window #586 using a 300 km window and the Tanaka method. B) The depth to the centroid of the magnetic source (Z_o) is calculated from the graph in the centre. C) The depth to the top of the magnetic source (Z_t) is calculated from the graph on the right. The red lines in B) and C) show the slopes that were used in the Z_o and Z_t calculations. The depth to the base of the magnetic source (Z_b; assumed to be the CPD) is calculated from: $Z_b = 2Z_o – Z_t$.*

As a second quality control step, we visually inspected and calculated a "goodness-of-fit" between the power spectra and the selected Z_o and Z_t lines used to determine CPD. A poor fit of the Z_o and Z_t lines tends to increase uncertainty in the calculated CPD value. As a measure of "goodness-of-fit," we calculated the r^2 value from a linear least squares regression of the power spectra data over the wavenumber ranges described above. Perfect fit yields an r^2 value of 1. The r^2 values for the 200 km windows range from 0.91 to 0.99. The r^2 values for the 300 km windows have a slightly wider range of 0.85 to 0.99. Overall the fit between the power spectra data and the Z_o and Z_t lines is moderately high to very high. We also created "CPD quality" maps which show combined RMS r^2 values for Z_o and Z_t for each window centre (Figs. 6 and 7). CPD quality is defined as:

CPD quality = $\sqrt{(0.5((r^2_{Zo})^2+(r^2_{Zt})^2)}$

where is the r^2_{Zo} value for Z_o and is the r^2_{Zt} value for Z_t.

RESULTS

The CPD estimates (*i.e.*, Z_b values) derived for all windows were plotted at the centre of each window and then contoured. This was done separately for the 200 km windows and the 300 km windows using both the Tanaka *et al.* (1999) and Bansal *et al.* (2011) methods.

The Curie point depth estimates derived with the Tanaka *et al.* (1999) method range from 25 to 42 km calculated on 200 km windows (Fig. 8) and 26 to 54 km using the 300 km windows (Fig. 9). The deepest CPD values (*i.e.*, >30 km) are located north of ~64° N latitude. Based upon CPD estimates from northeastern BC, the southeastern corner of Yukon is also inferred to have CPD values >30 km. By contrast, the south-central Yukon consists of a broad plateau with shallower CPD values of 25 to 30 km. A complete list of the Z_t, Z_o and Z_b values derived from the Tanaka method is presented in Appendices A and B.

The Curie point depth estimates derived using the Bansal *et al.* (2011) method are significantly shallower in south-central Yukon yet, in some cases, deeper elsewhere. CPD range from 5 to 19 km for 200 km windows and 3 to 83 km for 300 km windows. Similar to the results from the Tanaka *et al.* (1999) method, relatively deeper CPD values are found north of ~64° N latitude and in southeastern Yukon. South-central Yukon is characterized by CPD values of 5 to 10 km. CPD maps generated with the Bansal method are presented in Appendices C and D.

DISCUSSION

Regardless of the window size (200 km or 300 km) and irrespective of the method used (Tanaka or Bansal) the general trends in our results are remarkably similar. North of ~64° N and the southeastern corner of Yukon correspond to deeper CPD values. Likewise, south-central Yukon consistently exhibits shallower CPD estimates. Results obtained with 300 km windows in the far north and southeast are generally deeper than those using 200 km windows. This is likely a reflection of longer wavelength (deeper) signal obtained with the larger window size. The anomalously shallow CPD points found in the 200 km maps at 66° N and 138° W, which do not appear on the 300 km maps, are due to uncertainty in which wavelength range of the spectra to choose for calculating CPD. The power spectra recovered for the CPD windows in this area are of poor quality. Therefore, the accuracy of the CPD results in this part of northern Yukon is suspect. Similarly, we have low confidence in the accuracy of CPD estimates >50 km in the 300 km maps; the calculation windows are likely not large enough. Overall, the spatial distribution of CPD results suggests that, in general, mid-to-lower crustal temperatures in south-central Yukon should be higher compared to the northern and southeastern parts of the territory. By extension, crustal-scale temperature gradients in south-central Yukon are expected to be higher than in the rest of Yukon.

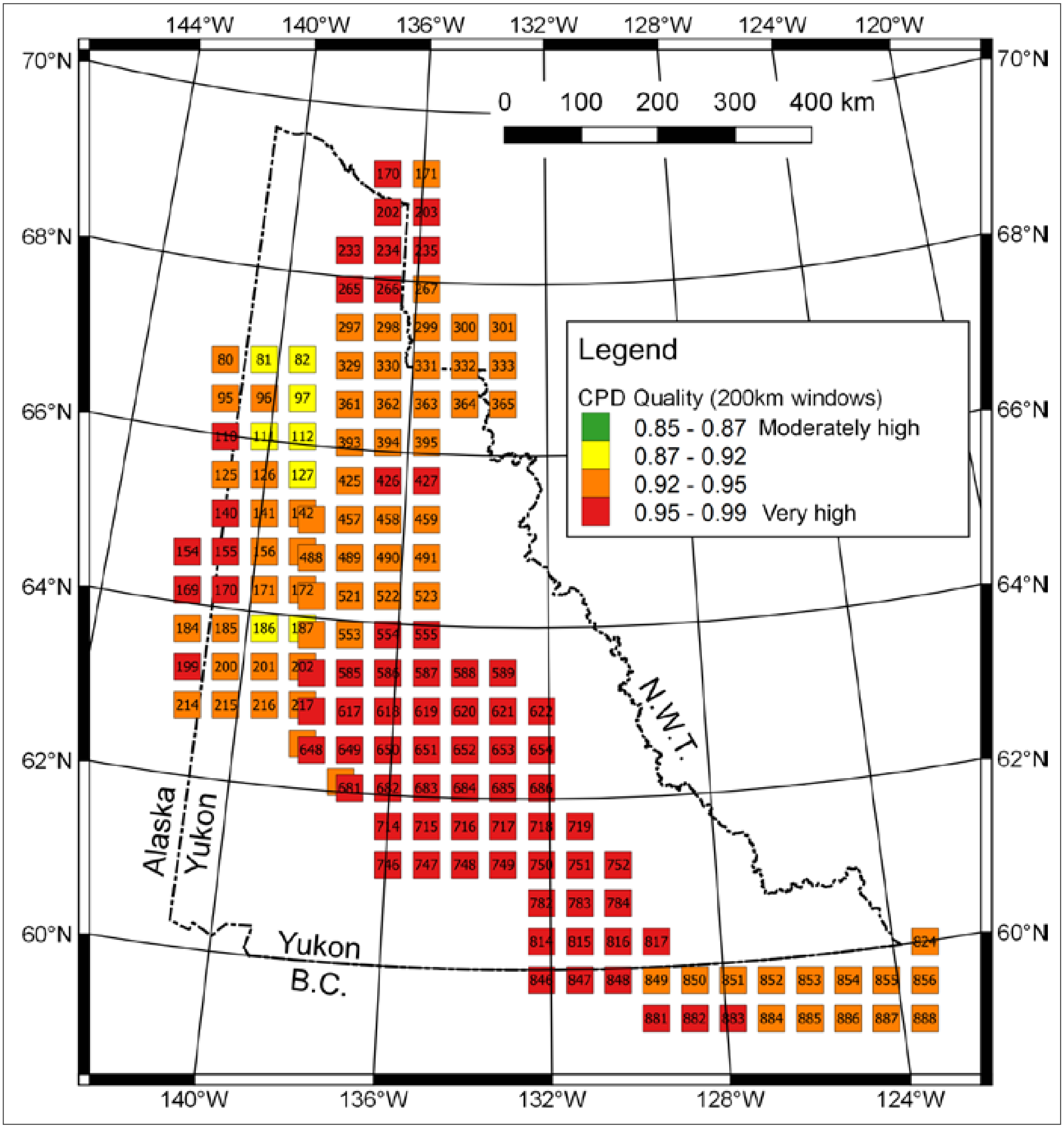

Figure 6. *Calculation quality map for the 200 km window CPD data. CPD was calculated for each 200 km window by fitting lines to spectra of the magnetic data. Depending on the window, the lines fit the spectra to a greater or lesser degree. Coloured boxes represent CPD windows that showed a very high degree of fit (red) and those that showed a moderately high degree of fit (green). Each coloured box is labelled with the window centre number.*

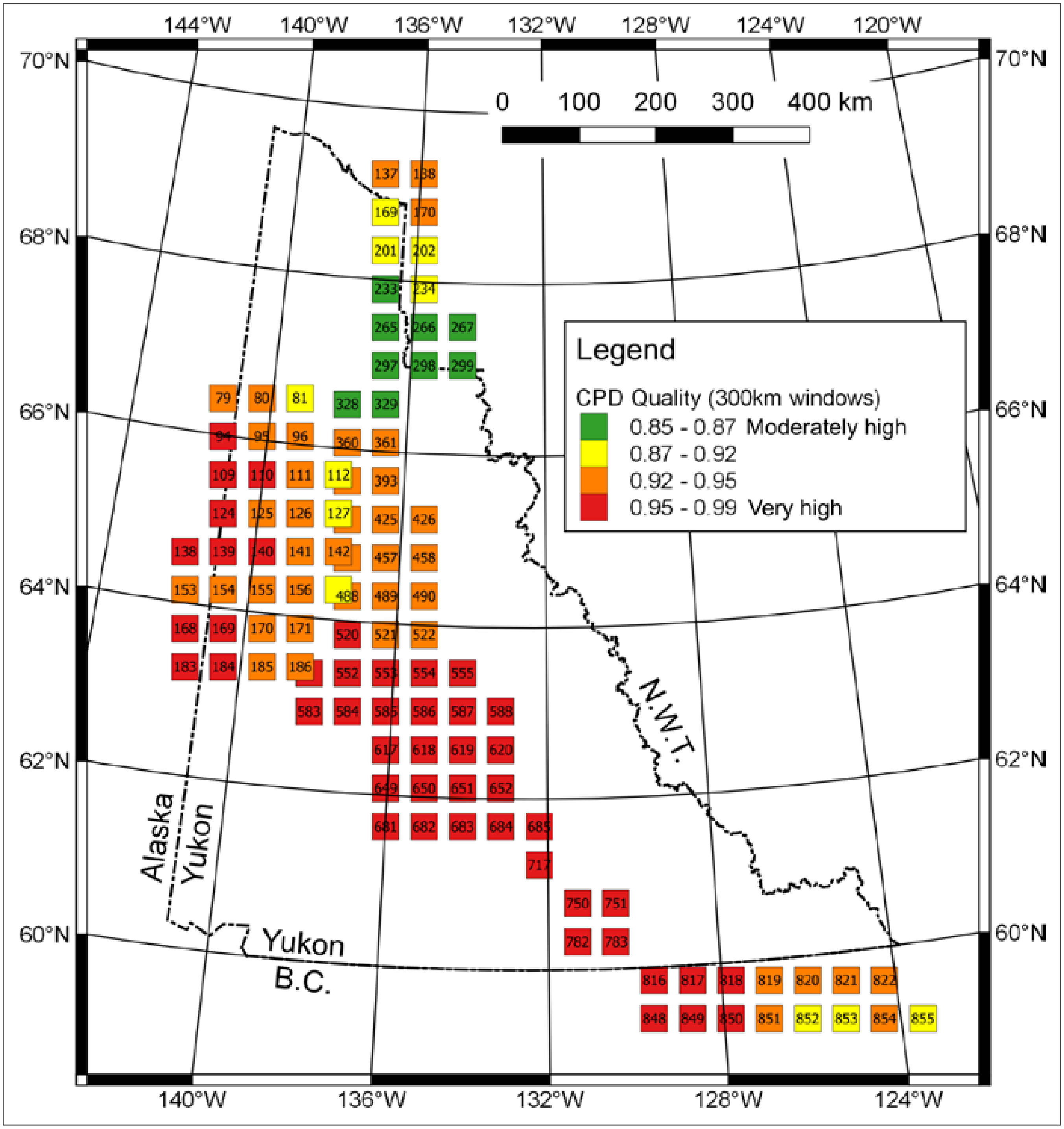

Figure 7. *Calculation quality map for the 300 km window CPD data. CPD was calculated for each 300 km window by fitting lines to spectra of the magnetic data. Depending on the window, the lines fit the spectra to a greater or lesser degree. Coloured boxes represent CPD windows that showed a very high degree of fit (red) and those that showed a moderately high degree of fit (green). Each coloured box is labelled with the window centre number.*

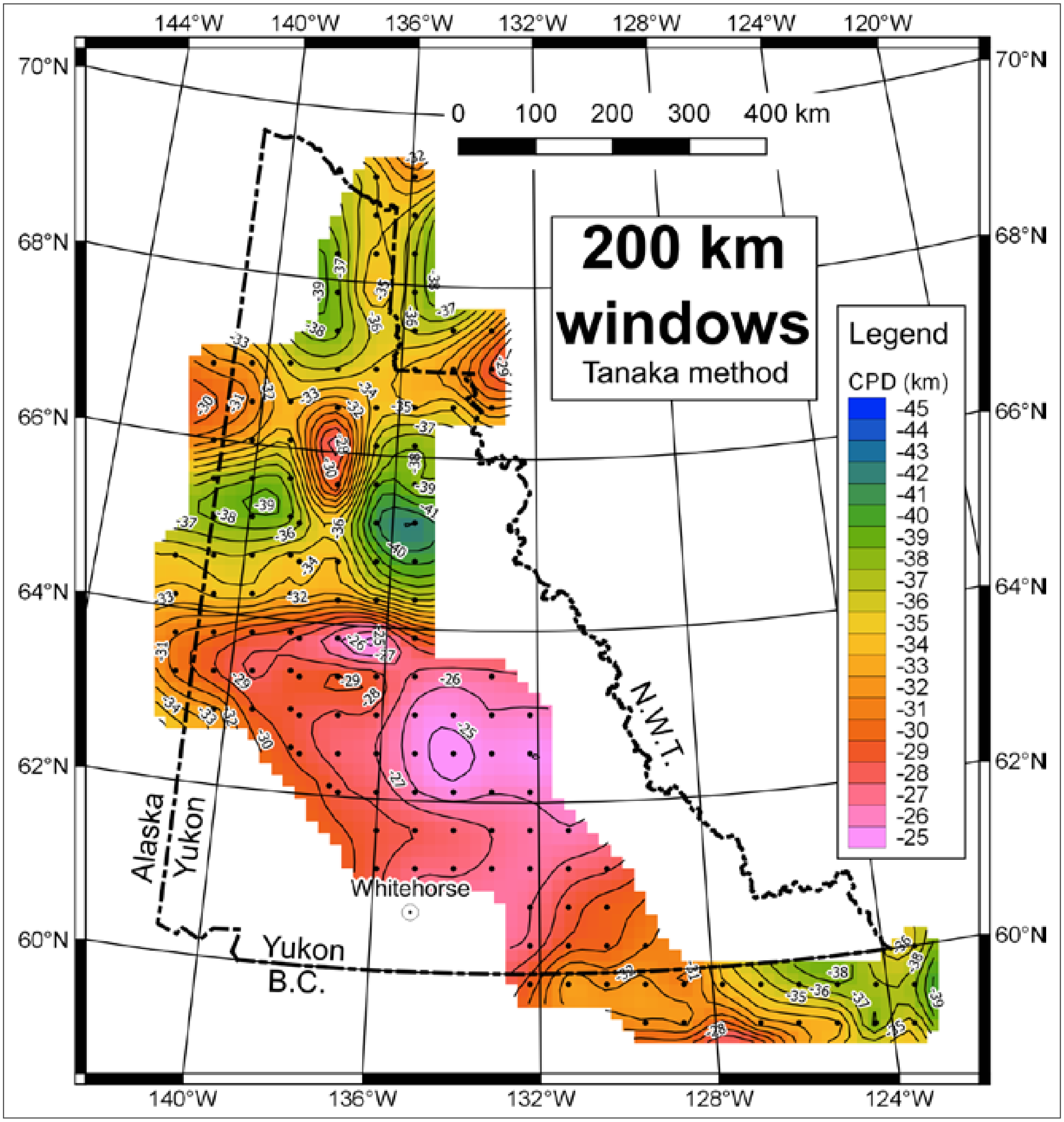

Figure 8. *Curie point depth map for Yukon using 200 km windows and the Tanaka et al. (1999) method. The window centres are shown as black dots. Warm and cool colours represent shallow and deep CPD estimates, respectively. Contour lines show CPD in units of kilometres below the surface.*

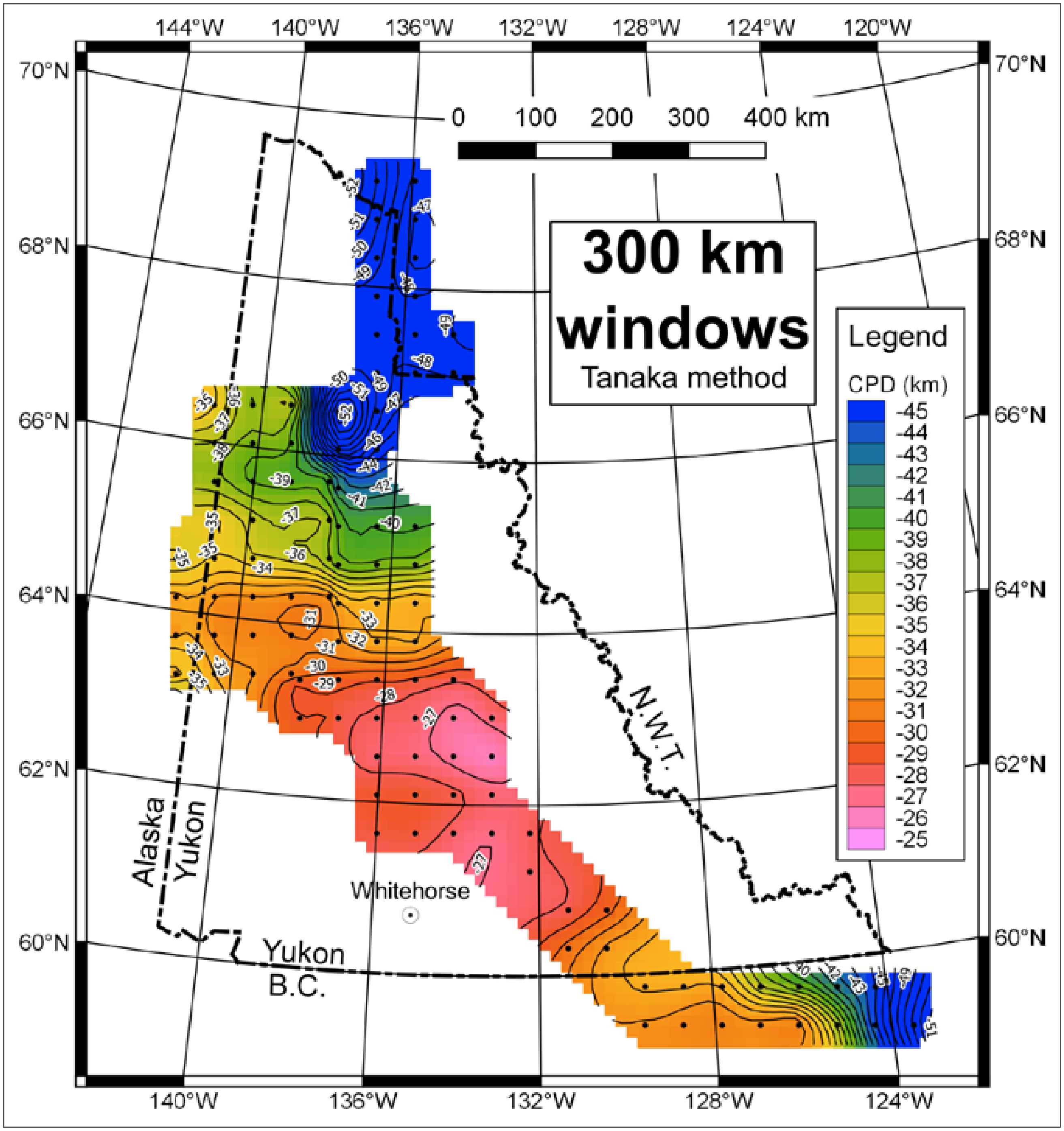

Figure 9. *Curie point depth map for Yukon using 300 km windows and the Tanaka et al. (1999) method. The window centres are shown as black dots. Warm and cool colours represent shallow and deep CPD estimates, respectively. Contour lines show CPD in units of kilometres below the surface.*

In order to capture the results of the Tanaka method into a single map, we created a composite CPD map (Fig. 10) which combines both the 200 km and 300 km CPD data points. Due to the larger window size, we have greater confidence in the accuracy of the 300 km CPD results. Therefore, 300 km CPD points are used in place of 200 km points in the composite map. In the northern and southeastern parts of Yukon, the 200 km windows likely do not contain sufficient long wavelength signal to resolve the deep (>35 km) CPD values in those areas. Thus, 200 km CPD values are not included in the composite map for northern and southeastern Yukon. In south-central Yukon, CPD values derived from 200 km and 300 km windows are similar and are likely shallow enough to be resolved with 200 km windows. Therefore, 200 km CPD points that lie outboard of the 300 km CPD points in south-central Yukon have been added to the composite map (Fig. 10).

Different Results from the Tanaka and Bansal Methods

The two CPD calculation methods employed in this study yielded similar results qualitatively (*i.e.*, locations of deep and shallow CPD), but the specific CPD values at a given location are quite different. The CPD results for Yukon using the Tanaka method are broadly similar to values obtained in other parts of the world. For example, Saibi *et al.*, (2015) found a CPD range of 16 to 40 km for Afghanistan. Trifonova *et al.* (2009) estimated CPD values of 28 to 32 km for the Moesian platform of central Bulgaria. Bansal *et al.* (2011) estimated the depth to the base of magnetic sources in Germany to have the range 22 to 45 km. In contrast, typical CPD values for areas of subduction zone volcanism and active volcanoes are commonly ~10 km or less (Tanaka *et al.*, 1999; De Ritis *et al.*, 2013). The lack of active volcanism in Yukon calls into question the validity of the shallow (<10 km) CPD results derived for Yukon using the Bansal method.

The Bansal method applies an approximate correction factor to the Tanaka method to account for fractal magnetization in the crust. Unfortunately, the Bansal method works up to a maximum fractal parameter value of $\beta = 2$ which may be too low for Yukon. The uncertainty in the fractal parameter value that we assumed ($\beta = 2$) in applying the Bansal method imparts significant ambiguity in the unusually shallow CPD results. Therefore, we choose not to further interpret or discuss the Bansal results in this report. Ongoing discussion of results refer to the CPD estimates obtained with the Tanaka method.

Comparison of CPD with Yukon Hot Springs and Volcanoes

Hot springs and recent volcanism are indicative of anomalous heat in the crust. In Figure 11, we compare the locations of hot springs and volcanism with the CPD composite map. Only two localities in Yukon show evidence for volcanic activity in the Holocene, the Alligator Lake volcanic complex (Eiche *et al.*, 1987) and Volcano Mountain in the Fort Selkirk volcanic field (Jackson and Stevens, 1992). Older, Neogene-to-Quaternary volcanism in Yukon is described in the vicinity of Alligator Lake and Fort Selkirk, as well as in the West Dawson region and near the town of Watson Lake (Edwards and Russell, 2000). None of these volcanic areas coincide with shallow CPD estimates (*e.g.*, ~10 km) as is found in other volcanic regions of the world (*e.g.*, De Ritis *et al.*, 2013). Thus, it is unlikely that recent volcanism in Yukon is a significant source of geothermal heat.

Hot springs in Yukon are located in areas with deep (~35 to 40 km) CPD (*e.g.*, Nash Creek, Pool Creek, and Larsen) as well as in regions with more moderate (~28 km) CPD estimates (*e.g.*, Takhini and McArthur). A consistent correlation between CPD values and hot springs is not evident. The heat required to feed hot springs can be generated by shallow crustal processes such as heat generation from radiogenic granites and/or heat accumulation under sedimentary caprocks. In addition, faults can act as vertical conduits for upward transport of hot water (causing hot springs). Thus, a lack of correlation between hot springs and CPD is not surprising.

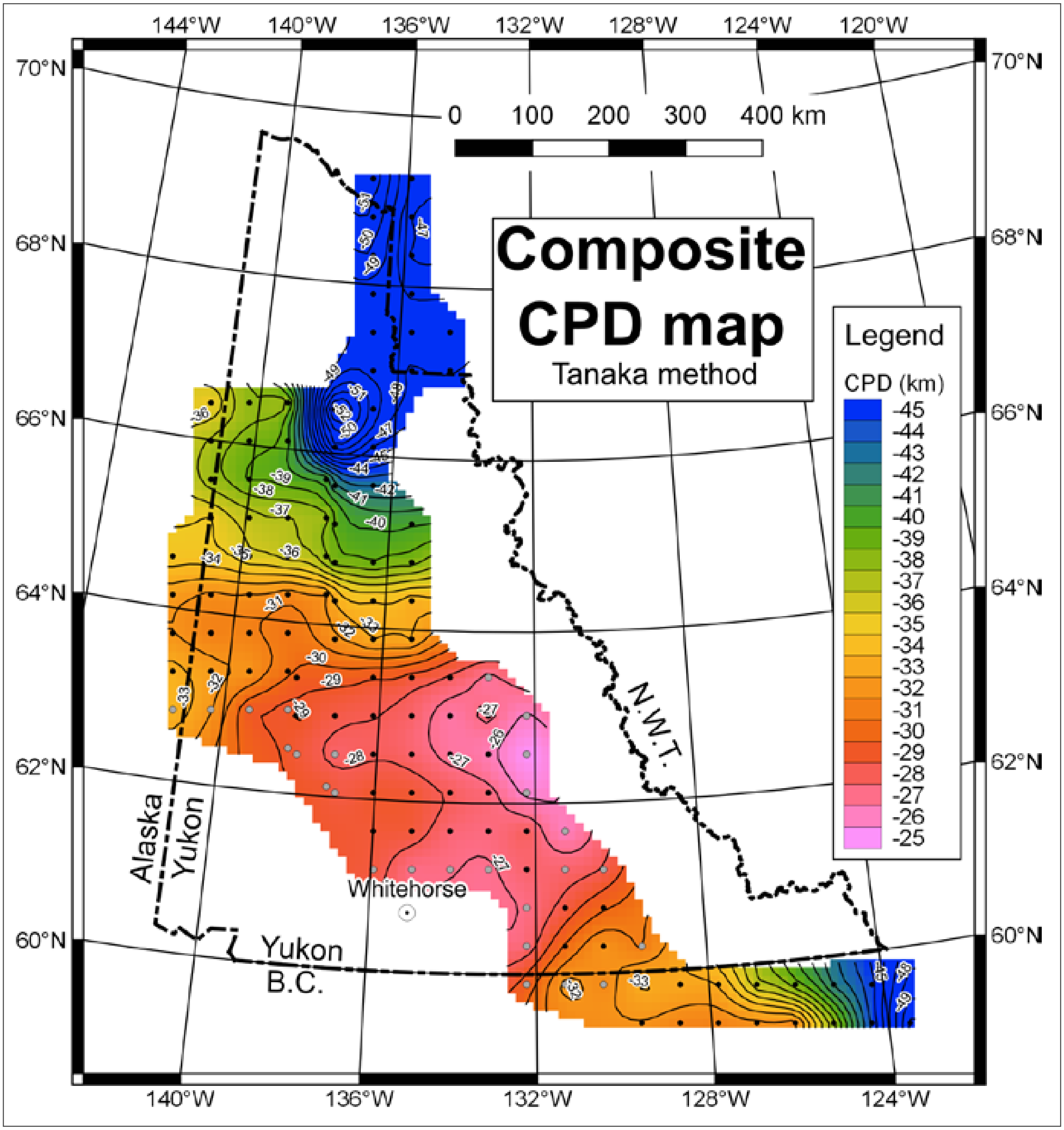

Figure 10. *Composite Curie point depth map for Yukon that combines results from both 200 km window CPD data (grey dots) and 300 km window CPD data (black dots) using the Tanaka et al. (1999) method. Warm and cool colours represent shallow and deep CPD estimates, respectively. Contour lines show CPD in units of kilometres below the surface.*

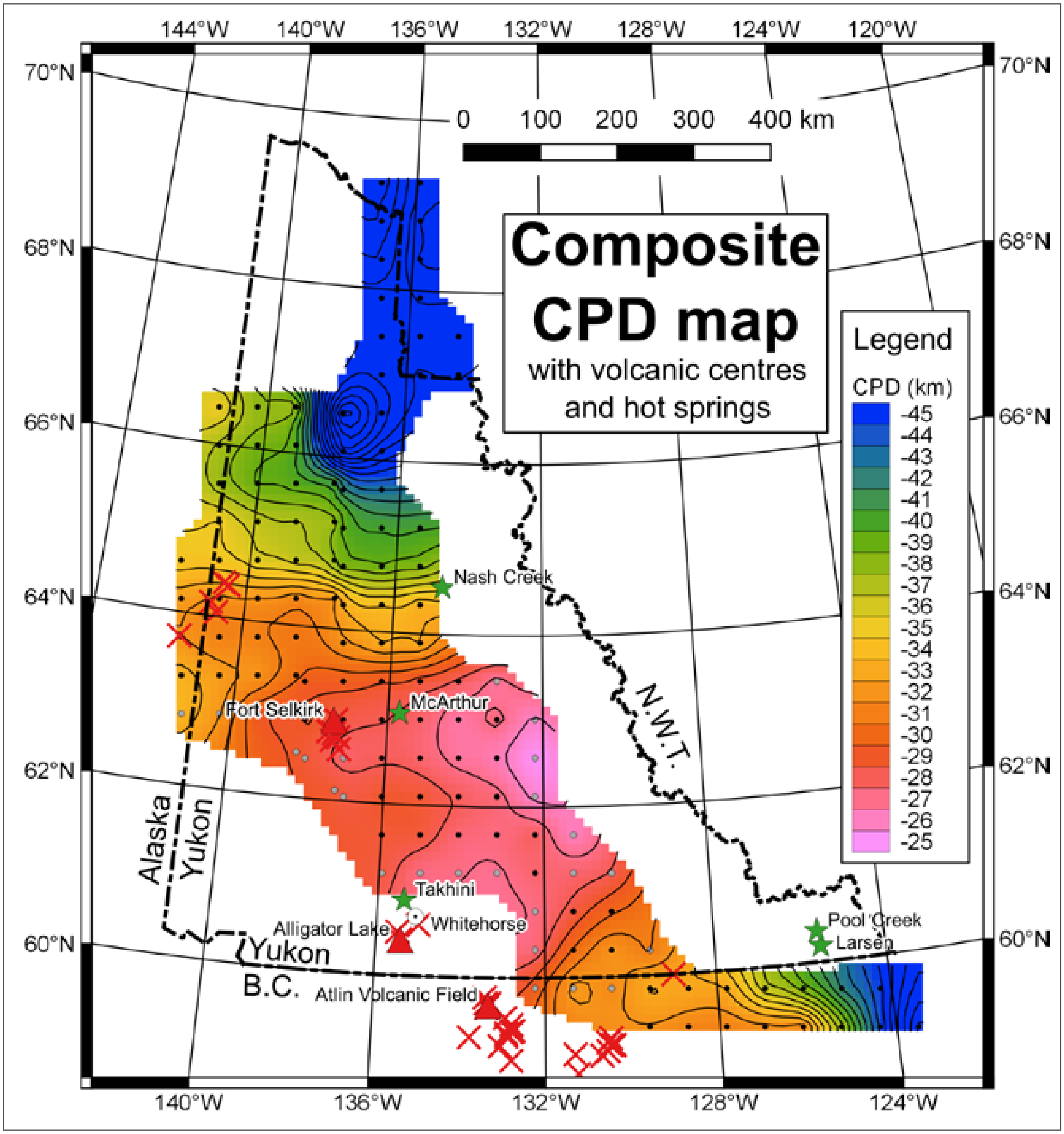

Figure 11. *Composite CPD map with regions of known volcanism and hot springs overlain. Hot springs are shown by green stars and labelled. Red triangles denote Holocene volcanic eruptions (Smithsonian, 2016); red crosses identify Neogene and younger volcanic rocks (Edwards and Russell, 2000).*

Comparison with Yukon Heat Flow

Figure 12 shows a map comparing Yukon heat flow with the CPD estimates. Although the heat flow data are sparse, the general trend is for lower heat flow values in Yukon's north and southeast (<70 mW/m^2) and higher heat flow across south-central Yukon (>80 mW/m^2). Lewis *et al.* (2003) provided evidence that heat flow in the northern Cordillera (north of 59° N) is 105 ± 22 mW/m^2. For comparison, the average heat flow for all of Canada is 64 ± 16 mW/m^2 (Grasby *et al.*, 2012). These general trends in heat flow agree well with CPD estimates. Specifically, the broad platform of 25 to 30 km CPD in south-central Yukon correlates with the region of high measured heat flow in the Cordillera. Similarly, the northern part and southeastern corner of Yukon, which exhibit relatively low heat flow, correspond to regions where CPD estimates drop to greater depths (*e.g.*, >30 km). Thus, in a qualitative sense, the correlation between CPD value and observed heat flow appears to be consistent.

An exception to the observed correlation is the heat flow measurement near Whitehorse. Lewis *et al.* (2003) report 60 mW/m^2, yet the CPD estimate for this area is relatively shallow at ~27 km. One hypothesis to explain this lower heat flow value is that the rocks of the Stikinia, Yukon-Tanana and Nisling terranes (which are thought to comprise the entire thickness of the crust under the Whitehorse area; Cook *et al.*, 2004) may have lower average heat generation values due to an abundance of mafic rocks containing lower concentrations of radioactive elements. Alternatively, the single heat flow measurement in Whitehorse may not be representative of the broader region. Regardless, the lack of a deeper CPD value in the vicinity of Whitehorse to match the modest heat flow measurement remains unexplained.

Comparison with Regional Geology and Major Faults

Yukon consists of a variety of crustal blocks broken by major fault zones (Fig. 13). In general, Yukon can be divided into the Arctic Alaska terrane (far northwestern corner of Yukon), Ancestral North America (northeast of the Tintina fault), and an assortment of displaced terranes (located mostly southwest of the Tintina fault). Variations in CPD estimates across Yukon do not appear to have a spatial association with these three geologic domains.

Significant northwest-trending faults are also found in Yukon (*e.g.*, Tintina, Teslin and Denali; Fig. 13). The distribution of CPD estimates do not appear to have any relationship with the major fault zones. For example, the broad region of moderate CPD values (25 to 30 km) in south-central Yukon extends across both the Tintina and Teslin fault zones.

The transition from shallow to deep CPD values observed in Yukon appears to instead coincide with the transition from deep water facies to platform facies in rocks belonging to Ancestral North America. The clearest example of this occurs at ~65° N where CPD values drop from <34 km in the south to >34 km to the north. At about this latitude, rocks transition from deep water Selwyn basin facies, in the south, to shelf facies of the Ogilvie Platform (*a.k.a.*, Yukon Stable Block) in the north (Nelson *et al.*, 2013). A second example of this relationship can be identified in the southeastern corner of Yukon where the transition to deep (>34 km) CPD values corresponds with the transition from Ancestral North America basinal facies and Intermontane rocks (to the west) and shelf facies of the MacDonald platform (to the east; Fig. 13). Regions with deeper CPD values suggest lower heat flow from the mid-to-lower crust. Thus, deep CPD values that correlate with Ancestral North American platform rocks may imply that: a) the platforms are composed of thicker, colder lithosphere and/or b) the crust in the platforms contains lower concentrations of radioactive, heat-generating elements. Either of these options would result in lower heat flow in the mid-to-lower crust, consistent with deep CPD values. Indeed, the southeastern corner of Yukon lies on the edge of the Wopmay orogen. Cook *et al.* (2012) argued that the Wopmay lithosphere is ~180 km thick compared to ~55 to 70 km thick for the Cordilleran lithosphere. Lewis *et al.* (2003) suggested that, although highly variable, the Wopmay orogen may also have lower heat generation values compared to the adjacent Cordillera. Similar features may characterize the Ogilvie platform.

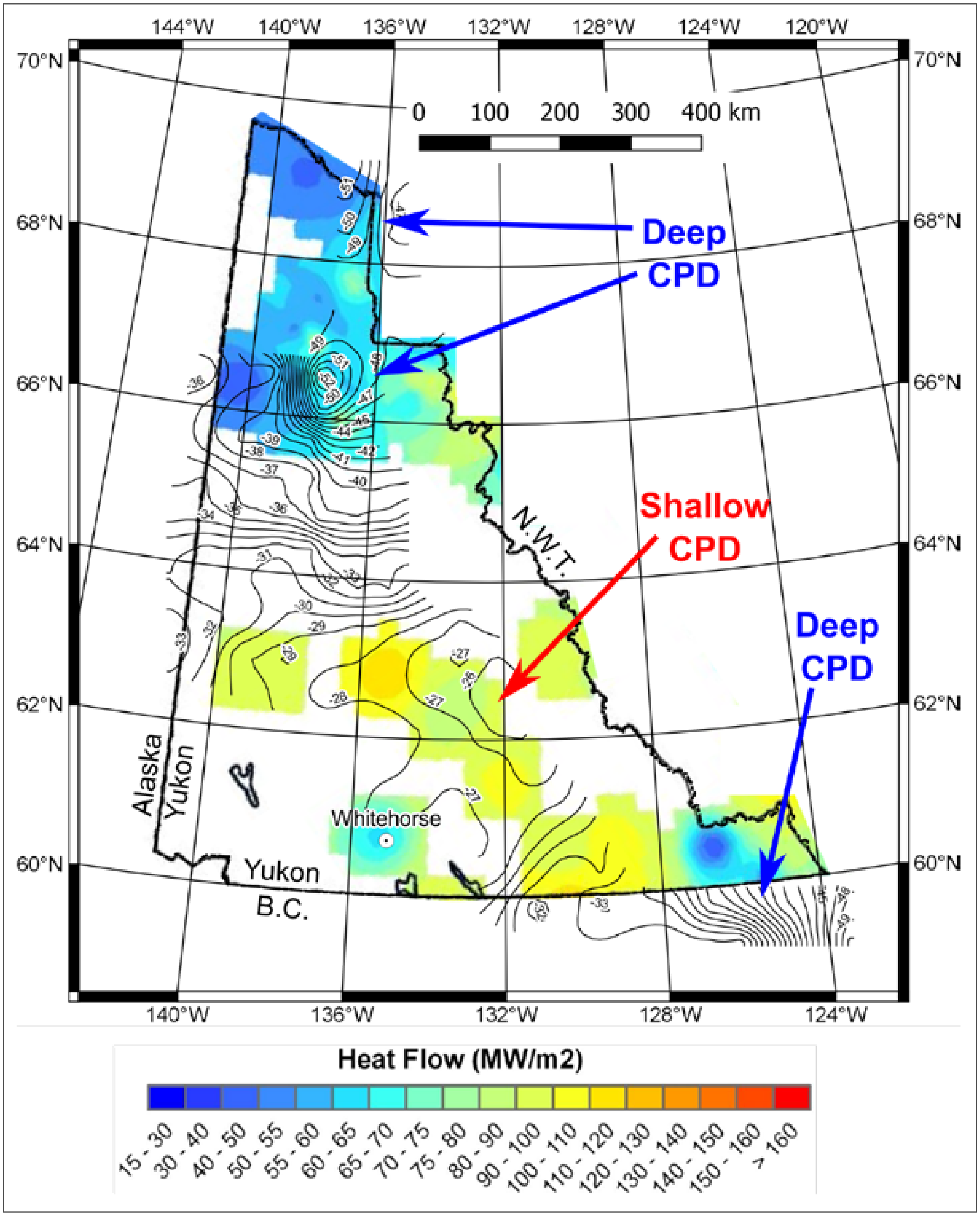

Figure 12. *Comparison between the heat flow map for Yukon (Grasby et al., 2012) and the composite CPD map generated in this study. The CPD contours are shown as black lines and labelled with depth in km. Heat flow is shown in the background with warm and cool colours representing high and low heat flow respectively.*

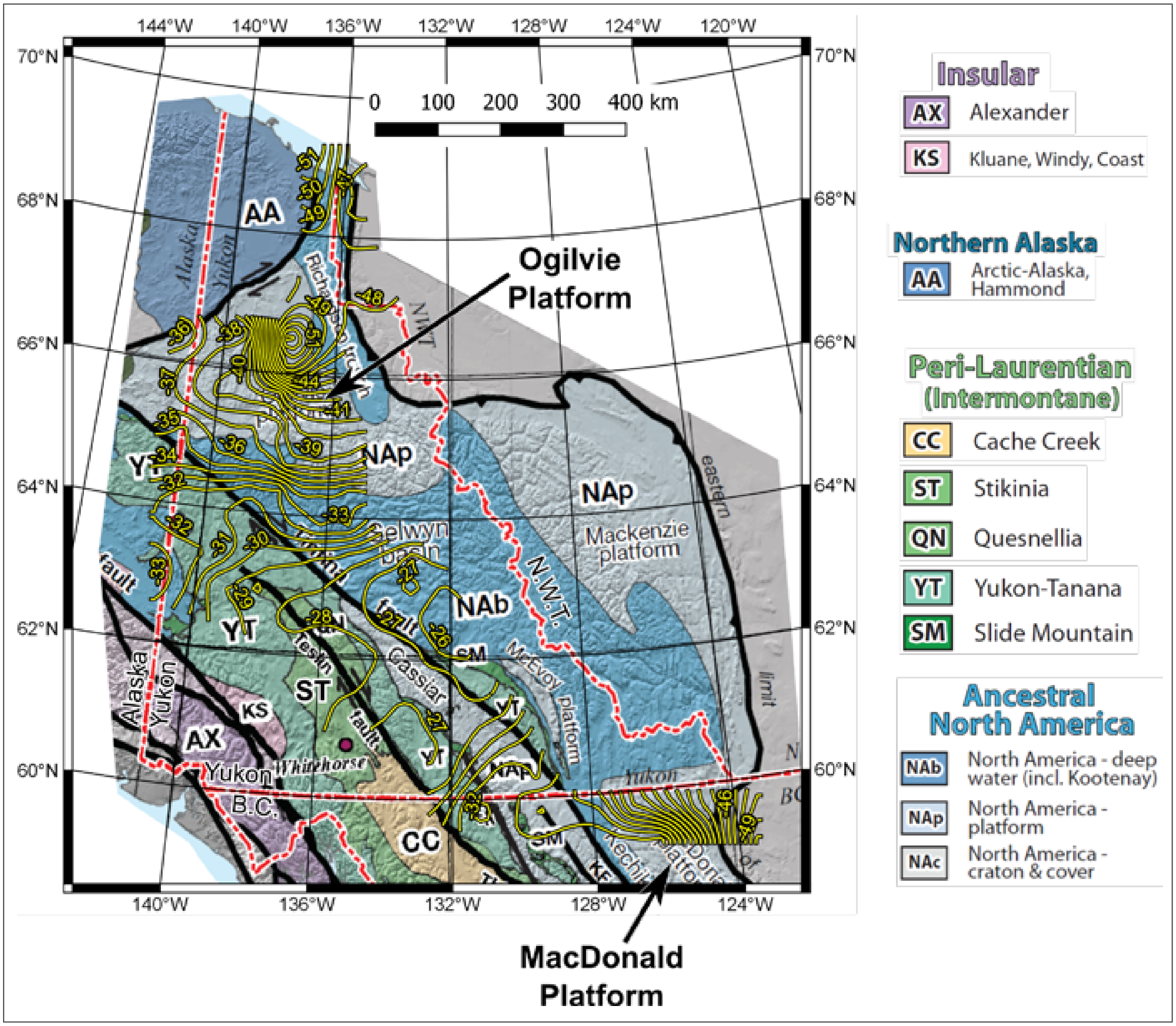

Figure 13. *Comparison between the regional geologic terrane map for Yukon (adapted from Nelson et al., 2013) and the composite CPD map generated in this study. The CPD contours are shown as yellow lines and labelled with yellow numbers showing depth in km. See text for discussion.*

Comparison with other Geotherms

If we assume that CPD estimates correspond to the Curie point temperature of 580°C and also assume a linear fall off of temperature with depth, we can roughly predict the geothermal gradient for an area for comparison with other gradients. For example, the broad region of moderate CPD values (25 to 30 km) in south-central Yukon would imply an average geothermal gradient of ~19 to 23°C/km. Assuming an average crustal thickness of 33 to 36 km for this area (Cook *et al.*, 2012) gives a temperature at the base of the crust of ~625 to 825°C.

Other studies predict higher temperatures at the base of the crust in the northern Cordillera. For example, seismic velocity data from the SNORCLE project (Clowes *et al.*, 2005) suggest temperatures at the base of the crust of 800 to 1000°C. Based upon a crustal heat flow model, Lewis *et al.* (2003) predict temperatures of 950±150°C at the base of the crust north of 59° N in Yukon. Similarly, Harder and Russell (2005) used geothermometry of mantle xenoliths to estimate a temperature of 800 to 850°C at the base of the crust beneath northernmost British Columbia near Atlin. A similar study of mantle xenoliths by Edwards and Russell (2000) suggest upper mantle temperatures of 950 to 1000°C beneath the Fort Selkirk and Alligator Lake volcanic fields in Yukon (these may not represent the temperature at the base of the crust, but more likely represent uppermost mantle temperatures).

Taken together, the results of seismic, heat flow and petrologic studies suggest the temperature at the base of the crust in the northern Cordillera is on the order of ~900°C with an average crustal-scale geothermal gradient of 25 to 27°C/km (assuming crustal thickness of 33 to 36 km). In comparison, the CPD estimates derived for the northern Cordillera in this study suggest a much lower temperature at the base of the crust (~625 to 825°C) and geothermal gradients that are similarly lower (~19 to 23°C/km). Reconciling this disparity is difficult.

To more rigorously compare our CPD estimates for south-central Yukon with these other datasets, we constructed a two-layer thermal model for the crust (Fig. 14) which mimics the crustal scale geology for the region (*e.g.*, Snyder *et al.*, 2002; Cook *et al.*, 2004). Specifically, the thermal model consists of an upper layer ~5 km thick (Paleozoic and younger rocks consisting of displaced terranes) underlain by a ~30 km thick layer of Proterozoic metasedimentary rocks of Ancestral North America. We utilize a steady-state conductive temperature model for a one-dimensional crustal lithosphere (Harder and Russell, 2005; Majorowicz and Grasby, 2010):

$$Q = Q_r + D\,A \qquad (2)$$

$$T(z) = T_0 + Q_r\,z\,K^{-1} + A\,D^2\,K^{-1}\,(1 - \exp(-z/D)) \qquad (3)$$

where Q is heat flow at the top of a crustal layer; Q_r = reduced heat flow at the base of a crustal layer; D = thickness of the crustal layer; A = heat generation in a crustal layer; T(z) is the temperature in the crustal layer as a function of depth; z = depth; T_0 = temperature at the top of a crustal layer; and K = thermal conductivity of a crustal layer. Estimates for values of thermal conductivity, heat generation, heat flow and temperature at the base of the crust (T_{Moho}) were derived from the literature (Table 1). There is uncertainty in the most appropriate values of K, A and Q to assign as bulk values for the two layers of the model. Therefore, we used average values and fixed the temperature of the land surface to 0°C (average annual temperature of Whitehorse). Our crustal-scale thermal model suggests that the Curie point (580°C) is reached at ~20 km (Fig. 14). Allowing for various values of K, A and Q, while still attaining the expected Moho temperature range of 800 to 1000°C, suggests the Curie point depth may range from 18 to 23 km. Reaching the Curie point at such depths implies an average linear temperature gradient of ~25 to 32°C/km between the surface and the mid-to-lower crust. If this thermal model is accurate then the CPD values obtained in this study (25 to 30 km) using the Tanaka *et al.* (1999) method are 2 to 12 km too deep for the south-central Yukon.

The cause of the discrepancy between the CPD estimates and geotherms derived from other data most likely has to do with the assumption of random magnetization in the crust. The Tanaka *et al.* (1999) method assumes random magnetization. Incorporating a fractal distribution of magnetization tends to make CPD estimates shallower. A shallower CPD estimate would bring it into agreement with geotherms derived from other data. Therefore, to make CPD estimation for Yukon more accurate and quantitative, a more advanced CPD methodology that appropriately incorporates fractal magnetization is needed. In addition, the appropriate fractal parameter (β) to use in CPD calculations for different regions of Yukon will need to be assessed.

Table 1. *List of variables used in the two-layer thermal model. The column marked 'Value' is the average assumed values used to calculate the black line in Figure 14. The column labelled 'Range' lists the variation in these variables found in the literature. PROT=Proterozoic metasedimentary rocks of Ancestral North America.*

DISPLACED TERRANE LAYER (0 - 5 KM)					
Variable	**Value**	**Range**	**Units**	**Description**	**Reference**
T_{surf}	0	n/a	°C	Temperature at land surface	assumed
Q_{surf}	105	105±22	mW/m²	Heat flow at land surface	Lewis *et al.* (2003)
$K_{terrane}$	3	2.6-3.4	W/m.K	Thermal conductivity in displaced terrane	Majorowicz and Grasby (2010); Lewis *et al.* (2003)
$A_{terrane}$	4	2.0-5.0	μW/m³	Heat generation in displaced terrane	Majorowicz and Grasby (2010); Lewis *et al.* (2003)
$D_{terrane}$	5	?	km	Thickness of displaced terrane	Snyder et al. (2002); Cook *et al.* (2004)
$Q_{terrane}$	85	n/a	mW/m²	Heat flow at base of displaced terrane	Calculated in this study
PROTEROZOIC ANCESTRAL NORTH AMERICA LAYER (5 - 35 KM)					
Variable	**Value**		**Units**	**Description**	**Reference**
T_{PROT}	163	n/a	°C	Temperature at top of Proterozoic rocks	Calculated in this study
K_{PROT}	2.7	1.8-3.4	W/m.K	Thermal conductivity of Proterozoic rocks	Majorowicz and Grasby (2010); Lewis *et al.* (2003)
A_{PROT}	1.5	0.9-3.7	μW/m³	Heat generation of Proterozoic rocks	Majorowicz and Grasby (2010); Lewis *et al.* (2003)
D_{PROT}	30	?	km	Thickness of Proterozoic rocks	Snyder *et al.* (2002); Cook *et al.* (2004)
Q_r	40	?	mW/m²	Reduced heat flow at base of crust	Harder and Russell (2005)
T_{Moho}	924	800-1000	°C	Temperature at base of crust	Calculated in this study; Clowes *et al.* (2005); Lewis *et al.* (2003)

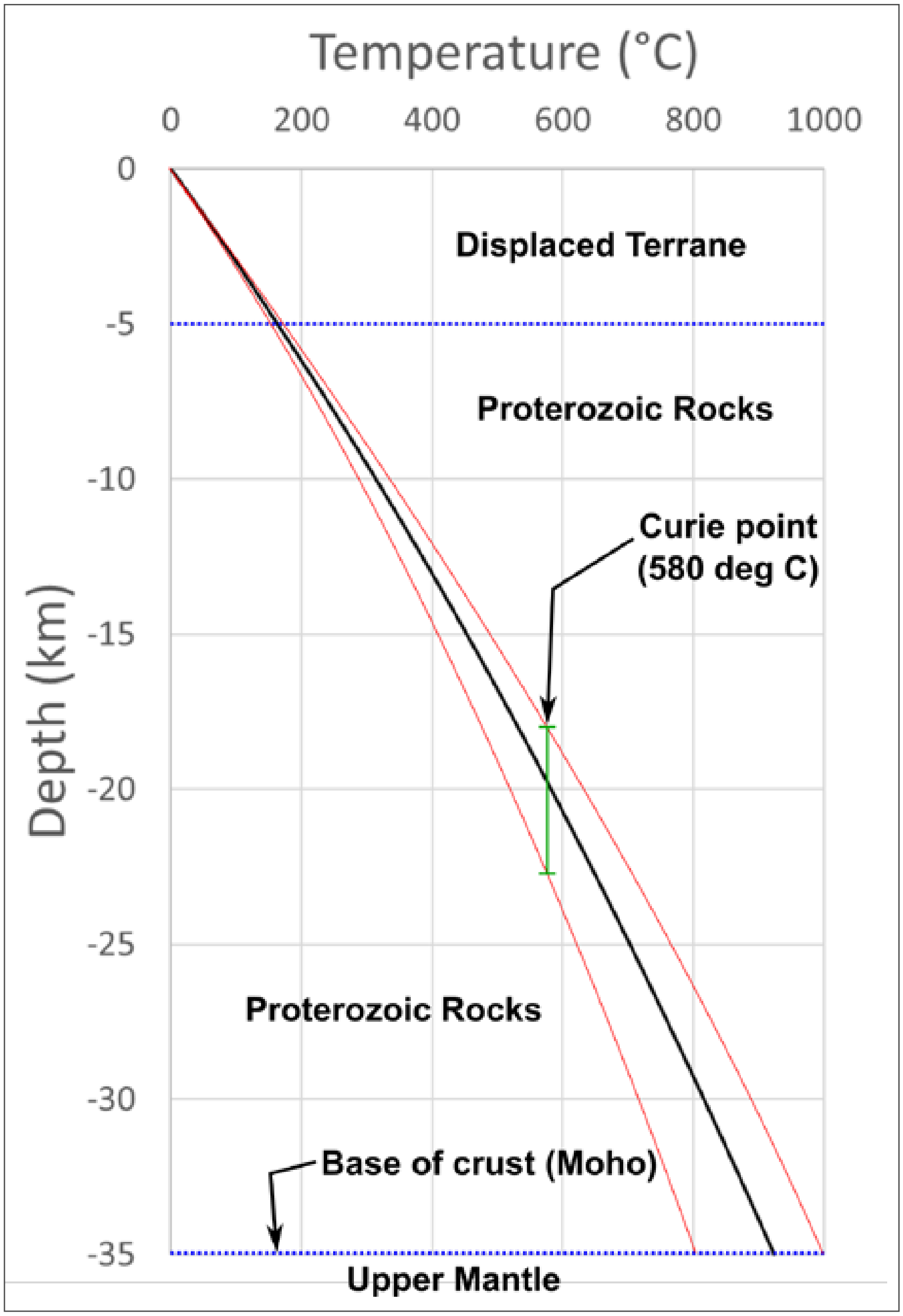

Figure 14. *Two-layer thermal model constructed for south-central Yukon. The geotherm calculated in this study (black line) uses the values in Table 1 and predicts a Curie point depth of ~20 km. Approximate bounding geotherms (red lines) to reach 800°C and 1000°C at the base of the crust suggest a range in Curie point depth of 18-23 km. See text for further explanation.*

CONCLUSIONS

In this study, we used two different Curie point depth mapping methods in an attempt to predict the depth to 580°C across Yukon. Based upon a comparison of our results with geothermal gradients predicted using other methods, we conclude that the CPD estimates derived from this study using the Tanaka *et al.* (1999) method are too deep. The reason for the discrepancy has to do with a key assumption of randomly distributed magnetic sources which may not be appropriate for Yukon. Nonetheless, the CPD results from this study are useful in a qualitative sense. Specifically, we have produced a map which covers the entire territory and demarcates regions where one would expect high and low average geothermal gradients in the Earth's crust (Fig. 15). The composite CPD map for Yukon used in conjunction with existing, sparse heat flow measurements can be used to infer average geothermal gradients in the territory. For example, the results from this study have identified a broad region of south-central Yukon that can be expected to have elevated geothermal gradients relative to other parts of Yukon. This region extends from ~64° N to the Yukon-BC border and from ~127° W to the Yukon-Alaska border. The region southwest of the Denali fault zone is not included in our assessment because it lies in a zone of no data outside of the CPD study area. This study also identified two parts of Yukon that can be expected to have lower average geothermal gradients, specifically, north of ~64° N and the southeastern corner of Yukon (east of ~127° W). These areas have deep CPD estimates and generally coincide with low measured heat flow.

CPD estimates from this study provide information on the relative heat flow in the mid-to-lower crust. As part of the search for geothermal heat in Yukon, the results of this study should be combined with data on temperatures in the upper crust. For example, heat generation and thermal insulation are important factors that can strongly influence temperatures in the uppermost few kilometres of the crust. Thus, the regions of Yukon most prospective for geothermal heat likely exhibit all three of the following factors:

A. lies within the zone of shallow CPD values (*i.e.*, elevated heat flow from the mid-to-lower crust);

B. contains shallow crustal rocks with high concentrations of radioactive elements (*i.e.*, high heat generation); and

C. capped by a thick succession of thermally-insulating sedimentary rocks.

Existing evidence suggests that parts of the Whitehorse trough exhibit at least two of these features (A and C). Heat generation in rocks that underlie the Whitehorse trough is uncertain but may be elevated based upon regional geology considerations (Lewis *et al.*, 2003; Grasby *et al.*, 2012).

Geothermal resources should not be entirely ruled out in regions with deep CPD values identified in this study. Even if the predicted CPD is deep, elevated subsurface temperatures may be found in warm aquifers insulated by thick successions of sedimentary rocks. In Yukon, deep sedimentary basins such as Eagle Plain and the Liard basin may have sufficiently thick thermally-insulating cap rock to generate such warm conditions despite lower thermal input from the mid-to-lower crust. In addition, regions with high heat generation that lie in the zones of inferred deep CPD may generate enough heat to warm subsurface aquifers locally.

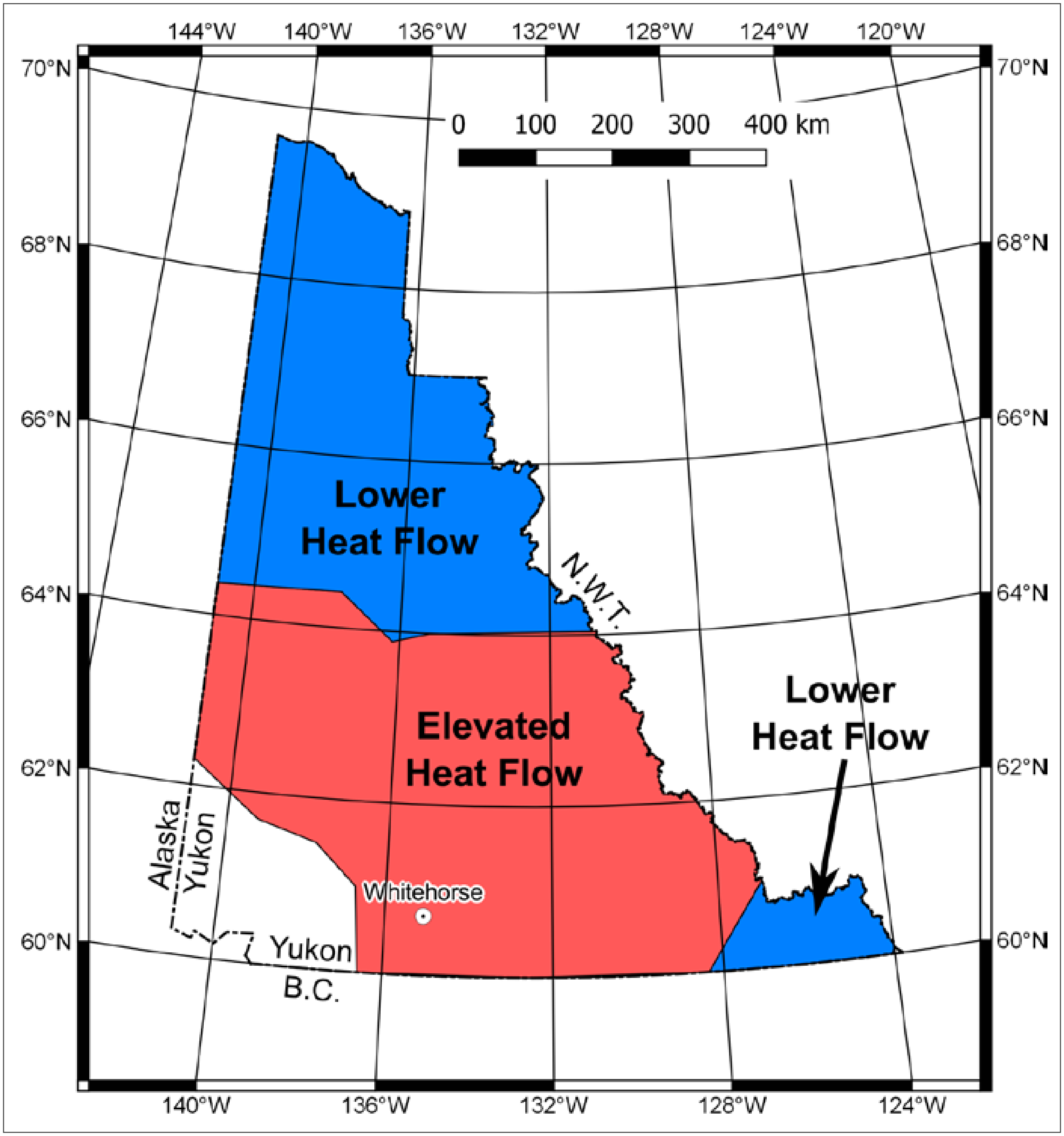

Figure 15. *Summary map from this CPD study. Yukon can be divided into regions with elevated heat flow in the mid-to-lower crust (south-central Yukon) and regions where heat flow in the mid-to-lower crust is expected to have lower values (southeastern Yukon and north of ~64° N).*

LIST OF DELIVERABLES

Filename	Description	Format
Yukon Curie point depth map report 2017.pdf	This report	.pdf
Yukon Curie point depth results 200km and 300km windows.xlsx	Spreadsheet listing the X, Y, and depth locations of the calculated Curie point depth estimates using the Tanaka *et al.* (1999) method	.xlsx
Yukon composite CPD contours.shp	Curie point depth map contour lines for the composite CPD map	.shp
Yukon composite CPD window centres.shp	Curie point depth data points used for the composite CPD map (located at the centres of the calculation windows)	.shp
Yukon composite CPD grid.tif	Composite Curie point depth map shown as gridded data	.tif and .tifw

All map-based deliverables are in Yukon Albers NAD83 coordinate system.

REFERENCES

Arnaiz-Rodriguez, M.S. and Orihuela, N., 2013. Curie point depth in Venezuela and the Eastern Caribbean. Tectonophysics, vol. 590, p. 38-51.

Aydin, I., Karat, H.I. and Koçak, A., 2005. Curie-point depth map of Turkey. Geophysical Journal International, vol. 162, p. 633-640.

Bansal, A.R., Gabriel, G., Dimri, V.P. and Krawczyk, C.M., 2011. Estimation of depth to the bottom of magnetic sources by a modified centroid method for fractal distribution of sources: An application to aeromagnetic data in Germany. Geophysics, vol. 76, no. 3, 10.1190/1.3560017.

Bhattacharyya, B.K. and Leu, L.-K., 1975. Analysis of Magnetic Anomalies Over Yellowstone National Park: Mapping of Curie Point Isothermal Surface for Geothermal Reconnaissance. Journal of Geophysical Research, vol. 80, no. 32, p. 4461-4465.

Bilim, F., Akay, T., Aydemir, A. and Kosaroglu, S. 2016. Curie point depth, heat-flow and radiogenic heat production deduced from the spectral analysis of the aeromagnetic data for geothermal investigation on the Menderes Massif and the Aegean Region, western Turkey. Geothermics, vol. 60, p. 44-57.

Blakely, R.J., 1988. Curie Temperature Isotherm Analysis and Tectonic Implications of Aeromagnetic Data from Nevada. Journal of Geophysical Research, vol. 93, no. B10, p. 11,817-11,832.

Bouligand, C., Glen, J.M.G. and Blakely, R.J., 2009. Mapping Curie temperature depth in the western United States with a fractal model for crustal magnetization. Journal of Geophysical Research, vol. 114, B11104, doi:10.1029/2009JB006494.

Campos-Enriquez, J.O., Arroyo-Esquivel, M.A. and Urrutia-Fucugauchi, J., 1990. Basement, curie isotherm and shallow crustal structure of the trans-Mexican volcanic belt, from aeromagnetic data. Tectonophysics, vol. 172, p. 77-90.

Chopping, R. and Kennett, B.L.N., 2015. Maximum depth of magnetisation of Australia, its uncertainty, and implications for Curie depth. GeoResJ, vol. 7, p. 70-77.

Clowes, R.M., Hammer, P.T.C., Fernandez-Viejo, G. and Welford, K., 2005. Lithospheric structure in northwestern Canada from Lithoprobe seismic refraction and related studies: a synthesis. Canadian Journal of Earth Sciences, vol. 42, p. 1277-1293.

Colpron, M. and Nelson, J.L., 2011. A Digital Atlas of Terranes for the Northern Cordillera. Accessed online from Yukon Geological Survey (www.geology.gov.yk.ca), December 1, 2016.

Connard, G., Couch, R. and Gemperle, M., 1983. Analysis of aeromagnetic measurements from the Cascade Range in central Oregon. Geophysics, vol. 48, no. 3, p. 376-390.

Cook, F.A., Clowes, R.M., Snyder, D.B., van der Velden, A.J., Hall, K.W., Erdmer, P. and Evenchick, C.A., 2004. Precambrian crust beneath the Mesozoic northern Canadian Cordillera discovered by Lithoprobe seismic reflection profiling. Tectonics, vol. 23, TC2010, doi:10.1029/2002TC001412.

Cook, F.A., Erdmer, P. and van der Velden, A.J., 2012. The evolving Cordilleran lithosphere. *In:* Tectonic Styles in Canada: the Lithoprobe perspective, J.A. Percival, F.A. Cook and R.M. Clowes (eds.), Geological Association of Canada, Special Paper 49, p. 1-39.

DeRitis, R., Ravat, D., Ventura, G. and Chiappini, M., 2013. Curie isotherm depth from aeromagnetic data constraining shallow heat source depths in the central Aeolian Ridge (Southern Tyrrhenian Sea, Italy). Bulletin of Volcanology, vol. 75, no. 4, p. 710, DOI 10.1007/s00445-013-0710-9.

Edwards, B.R. and Russell, J.K., 2000. Distribution, nature, and origin of Neogene – Quaternary magmatism in the northern Cordilleran volcanic province, Canada. GSA Bulletin, vol. 112, no. 8, p. 1280-1295.

Eiche, G.E., Francis, D.M. and Ludden, J.N., 1987. Primary alkaline magmas associated with the Quaternary Alligator Lake volcanic complex, Yukon Territory, Canada. Contributions Mineralogy Petrology, vol. 95, no. 2, p. 191-201.

Espinosa-Cardeña, J.M. and Campos-Enriquez, J.O., 2008. Curie point depth from spectral analysis of aeromagnetic data from Cerro Prieto geothermal area, Baja California, México. Journal of Volcanology and Geothermal Research, vol. 176, p. 601-609.

Grasby, S.E., Allen, D.M., Bell, S., Chen, Z., Ferguson, G., Jessop, A., Kelman, M., Ko, M., Majorowicz, J., Moore, M., Raymond, J. and Therrien, R., 2012. Geothermal Energy Resource Potential of Canada. Geological Survey of Canada, Open File 6914, 322 p.

Harder, M. and Russell, J.K., 2006. Thermal state of the upper mantle beneath the Northern Cordilleran Volcanic Province (NCVP), British Columbia, Canada. Lithos, vol. 87, p. 1-22.

Hseih, H.-H., Chen, C.-H., Lin, P.-Y. and Yen, H.-Y., 2014. Curie point depth from spectral analysis of magnetic data in Taiwan. Journal of Asian Earth Sciences, vol. 90, p. 26-33.

Jackson, L.E. and Stevens, W., 1992. A recent eruptive history of Volcano Mountain, Yukon Territory. Geological Survey of Canada, Paper 92-1A, p. 33-39.

Lewis, T.J., Hyndman, R.D. and Flück, P., 2003. Heat flow, heat generation, and crustal temperatures in the northern Canadian Cordillera: Thermal control of tectonics. Journal of Geophysical Research, vol. 108, no. B6, 2316, doi:10.1029/2002JB002090.

Majorowicz, J. and Grasby, S.E., 2010. Heat flow, depth-temperature variations and stored thermal energy for enhanced geothermal system in Canada. Journal of Geophysics and Engineering, vol. 7, p. 232-241.

Manea, M. and Manea, V.C., 2011. Curie Point Depth Estimates and Correlation with Subduction in Mexico. Pure and Applied Geophysics, vol. 168, p. 1489-1499.

Maus, S., Gordon, D. and Fairhead, D., 1997. Curie temperature depth estimation using a self-similar magnetization model. Geophysical Journal International, vol. 129, p. 163-168, doi:10.1111/j.1365-246X.1997.tb00945.x.

Nelson, J.L., Colpron, M. and Israel, S., 2013. The Cordillera of British Columbia, Yukon, and Alaska: Tectonics and Metallogeny. *In:* Tectonics, Metallogeny, and Discovery: The North American Cordillera and Similar Accretionary Settings, M. Colpron, T. Bissig, B.G. Rusk and J.F.H. Thompson (eds.), Society of Economic Geologists, Special Publication 17, p. 53-109.

Nyabeze, P.K. and Gwavava, O., 2016. Investigating heat and magnetic source depths in the Soutpansberg Basin, South Africa: exploring the Soutpansberg Basin Geothermal Field. Geothermal Energy, vol. 4, no. 8, 20 p.

Okubo, Y., Graf, R.J., Hansen, R.O., Ogawa, K. and Tsu, H., 1985. Curie point depths of the island of Kyushu and surrounding areas, Japan. Geophysics, vol. 53, no. 3, p. 481-494.

Okubo, Y., Tsu, H. and Ogawa, K., 1989. Estimation of Curie point temperature and geothermal structure of island arcs of Japan. Tectonophysics, vol. 159, p. 279-290.

Pilkington, M. and Todoeschuck, J.P., 1993. Fractal magnetization of continental crust. Geophysical Research Letters, vol. 20, p. 627-630, doi:10.1029/92GL03009.

Pilkington, M., Snyder, D.B. and Hemant, K., 2006. Weakly magnetic crust in the Canadian Cordillera. Earth and Planetary Science Letters, vol. 248, p. 476-485.

Ravat, D., Pignatelli, A., Nicolosi, I. and Chiappini, M., 2007. A study of spectral methods of estimating the depth to the bottom of magnetic sources from near-surface magnetic anomaly data. Geophysical Journal International, vol. 169, p. 421-434.

Saada, S.A., 2016. Curie point depth and heat flow from spectral analysis of aeromagnetic data over the northern part of Western Desert, Egypt. Journal of Applied Geophysics, vol. 134, p. 100-111.

Saibi, H., Aboud, E. and Azizi, M., 2015. Curie Point Depth Map for Western Afghanistan Deduced from the Analysis of Aeromagnetic Data. Proceedings World Geothermal Congress, Melbourne, Australia, 19-25 April, 12 p.

Shuey, R.T., Schellinger, D.K., Tripp, A.C. and Alley, L.B., 1977. Curie depth determination from aeromagnetic spectra. Geophysical Journal of the Royal Astronomical Society, vol. 50, p. 75-101.

Smithsonian Institution, 2016. Smithsonian Institution Global Volcanism Program Google Earth placemarks. Smithsonian Institution, http://volcano.si.edu/, accessed December 15, 2016.

Snyder, D.B., Clowes, R.M., Cook, F.A., Erdmer, P., Evenchick, C.A., van der Velden, A.J. and Hall, K.W., 2002. Proterozoic Prism Arrests Suspect Terranes: Insights into the Ancient Cordilleran Margin from Seismic Reflection Data. GSA Today, vol. 12, no. 10, p. 4- 10.

Spector, A. and Grant, F.S., 1970. Statistical Models for Interpreting Aeromagnetic Data. Geophysics, vol. 35, no. 2, p. 293-302.

Tanaka, A., Okubo, Y. and Matsubayashi, O., 1999. Curie point depth based on spectrum analysis of the magnetic anomaly data in East and Southeast Asia. Tectonophysics, vol. 306, p. 461-470.

Trifonova, P., Zhelev, Zh., Petrova, T. and Bojadgieva, K., 2009. Curie point depths of Bulgarian territory inferred from geomagnetic observations and its correlation with regional thermal structure and seismicity. Tectonophysics, vol. 473, p. 362-374.

Vacquier, V. and Affleck, J., 1941. A computation of the average depth to the bottom of the earth's magnetic crust, based on a statistical study of local magnetic anomalies. Transactions of the American Geophysical Union, 22nd Annual Meeting, p. 446-450.

Appendix A. List of Zo, Zt, and Zb values, Tanaka method 200 km windows

Window	Location (Yukon Albers NAD83)		Centroid depth	Centroid depth	Top depth	Top depth	Base depth	Base depth
	Easting (m)	Northing (m)	Z_o (km)	error (km)	Z_t (km)	error (km)	Z_b (km)	error (km)
80	103532	1406200	-18.28	1.08	-4.76	0.07	-31.81	1.08
81	153543	1406200	-18.79	1.18	-4.98	0.1	-32.6	1.18
82	203555	1406200	-20.63	1.15	-5.59	0.12	-35.67	1.16
95	103532	1356189	-17.49	0.94	-4.99	0.06	-29.98	0.94
96	153543	1356189	-18.27	1.04	-5.32	0.09	-31.23	1.05
97	203555	1356189	-19.88	1.15	-5.63	0.11	-34.13	1.16
110	103532	1306178	-18.65	0.84	-4.98	0.06	-32.33	0.84
111	153543	1306178	-19.83	1.14	-6.14	0.15	-33.51	1.15
112	203555	1306178	-20.54	1.21	-6.15	0.16	-34.93	1.22
125	103532	1256166	-20.58	0.71	-4.01	0.13	-37.14	0.73
126	153543	1256166	-20.99	0.81	-4.04	0.12	-37.94	0.82
127	203555	1256166	-21	1.12	-4.58	0.11	-37.41	1.13
140	103532	1206255	-20.08	0.81	-1.76	0.03	-38.4	0.81
141	153543	1206255	-20.4	0.93	-1.78	0.02	-39.02	0.93
142	203555	1206255	-20.22	1.19	-1.93	0.03	-38.51	1.19
154	53521	1156244	-18.12	0.74	-1.57	0.02	-34.67	0.74
155	103532	1156244	-18.58	0.79	-1.56	0.02	-35.61	0.79
156	153543	1156244	-18.55	0.86	-1.58	0.02	-35.53	0.86
157	203555	1156244	-18.06	1.04	-1.74	0.02	-34.38	1.04
169	53521	1106233	-17.53	0.75	-1.47	0.02	-33.58	0.75
170	103532	1106233	-17.89	0.8	-1.42	0.02	-34.37	0.8
170	315012	1648023	-22.11	0.94	-8.73	0.05	-35.48	0.94
171	153543	1106233	-17.96	0.84	-1.38	0.02	-34.53	0.84
171	365012	1648023	-20.61	1	-8.89	0.14	-32.32	1.01
172	203555	1106233	-17.42	1.01	-1.57	0.02	-33.27	1.01
184	53521	1056221	-16.36	0.84	-1.38	0.02	-31.34	0.84
185	103532	1056221	-15.91	0.88	-1.36	0.02	-30.47	0.88
186	153543	1056221	-15.41	0.88	-1.4	0.03	-29.43	0.88
187	203555	1056221	-15.21	0.9	-1.48	0.03	-28.95	0.9
199	53521	1006210	-16.4	0.59	-1.62	0.03	-31.18	0.59
200	103532	1006210	-15.3	0.77	-1.52	0.03	-29.08	0.77
201	153543	1006210	-14.73	0.67	-1.56	0.03	-27.89	0.67
202	203555	1006210	-15.28	0.67	-1.69	0.03	-28.87	0.67
202	315012	1598023	-22.05	0.96	-8.9	0.04	-35.2	0.96
203	365012	1598023	-22.41	0.96	-9.38	0.08	-35.44	0.96
214	53521	956199	-17.8	0.68	-1.96	0.04	-33.63	0.69
215	103532	956199	-16.9	0.8	-1.67	0.03	-32.13	0.8
216	153543	956199	-15.34	0.71	-1.61	0.02	-29.07	0.71

Appendix A continued.

Window	Location (Yukon Albers NAD83)		Centroid depth	Centroid depth	Top depth	Top depth	Base depth	Base depth
	Easting (m)	Northing (m)	Z_o (km)	error (km)	Z_t (km)	error (km)	Z_b (km)	error (km)
217	203555	956199	-15.17	0.66	-1.64	0.03	-28.7	0.66
232	203555	906187	-15.28	0.68	-1.69	0.03	-28.88	0.68
233	265012	1548023	-24.15	1.09	-9.84	0.04	-38.47	1.09
234	315012	1548023	-22.7	1	-10.48	0.15	-34.91	1.01
235	365012	1548023	-23.77	0.96	-10.34	0.23	-37.19	0.99
248	253566	856176	-15.31	0.71	-1.8	0.03	-28.83	0.71
265	265012	1498023	-24.32	1.09	-10.1	0.14	-38.54	1.1
266	315012	1498023	-22.5	0.98	-10.74	0.19	-34.26	1
267	365012	1498023	-24.02	1.02	-10.8	0.29	-37.24	1.06
297	265012	1448023	-24.6	1.04	-10.77	0.29	-38.44	1.08
298	315012	1448023	-23.39	1.08	-10.91	0.25	-35.88	1.11
299	365012	1448023	-23.75	1.08	-10.96	0.28	-36.54	1.11
300	415012	1448023	-23.52	1.09	-10.96	0.27	-36.09	1.12
301	465012	1448023	-21.94	1.15	-10.82	0.1	-33.06	1.15
329	265012	1398023	-23.48	1.07	-11.29	0.28	-35.67	1.1
330	315012	1398023	-22.91	1.12	-11	0.22	-34.82	1.14
331	365012	1398023	-22.32	1.14	-11.27	0.19	-33.37	1.16
332	415012	1398023	-21.83	1.12	-11.37	0.18	-32.29	1.13
333	465012	1398023	-20.26	1.19	-11.43	0.13	-29.1	1.2
361	265012	1348023	-21.72	1.08	-11.88	0.26	-31.56	1.11
362	315012	1348023	-22.67	1.17	-11.19	0.2	-34.14	1.18
363	365012	1348023	-22.68	1.12	-11.39	0.23	-33.97	1.14
364	415012	1348023	-23.1	1.13	-11.39	0.26	-34.81	1.16
365	465012	1348023	-21.67	1.15	-11.39	0.14	-31.96	1.16
393	265012	1298023	-19.77	1.06	-12.23	0.17	-27.3	1.07
394	315012	1298023	-23.01	1.25	-10.53	0.13	-35.49	1.26
395	365012	1298023	-24.31	1.12	-10.85	0.29	-37.77	1.16
425	265012	1248023	-19.58	0.97	-9.49	0.13	-29.66	0.98
426	315012	1248023	-23.45	1.2	-8.21	0.06	-38.69	1.2
427	365012	1248023	-23.08	1.17	-8.01	0.07	-38.15	1.17
456	215012	1198023	-20.59	1.04	-4.17	0.03	-37.01	1.04
457	265012	1198023	-19.74	0.98	-4.3	0.04	-35.18	0.98
458	315012	1198023	-22.51	1.15	-4.63	0.07	-40.4	1.15
459	365012	1198023	-23.41	1.1	-4.85	0.09	-41.97	1.11
488	215012	1148023	-19.35	0.99	-4.11	0.03	-34.59	0.99
489	265012	1148023	-19.08	0.96	-4.24	0.03	-33.93	0.96
490	315012	1148023	-21.29	1.17	-4.51	0.05	-38.07	1.17
491	365012	1148023	-22.45	1.13	-4.57	0.05	-40.33	1.13

Appendix A continued.

Window	Location (Yukon Albers NAD83)		Centroid depth	Centroid depth	Top depth	Top depth	Base depth	Base depth
	Easting (m)	Northing (m)	Z_o (km)	error (km)	Z_t (km)	error (km)	Z_b (km)	error (km)
520	215012	1098023	-18.86	0.97	-4.05	0.03	-33.66	0.97
521	265012	1098023	-18.54	0.94	-4.14	0.03	-32.95	0.94
522	315012	1098023	-19.71	1.05	-4.42	0.04	-35	1.05
523	365012	1098023	-20.85	1.14	-4.59	0.05	-37.1	1.14
552	215012	1048023	-15.8	0.79	-4.06	0.03	-27.55	0.79
553	265012	1048023	-15.25	0.75	-4.29	0.03	-26.22	0.75
554	315012	1048023	-14.58	0.61	-4.51	0.04	-24.64	0.62
555	365012	1048023	-16.62	0.78	-4.47	0.04	-28.76	0.78
584	215012	998023	-16.55	0.63	-4.22	0.04	-28.88	0.63
585	265012	998023	-16.75	0.68	-4.38	0.03	-29.11	0.68
586	315012	998023	-16.69	0.65	-4.57	0.04	-28.81	0.65
587	365012	998023	-15.63	0.72	-4.44	0.03	-26.81	0.72
588	415012	998023	-15.39	0.71	-4.35	0.03	-26.43	0.71
589	465012	998023	-15.49	0.67	-4.32	0.03	-26.65	0.67
616	215012	948023	-16.3	0.64	-4.31	0.04	-28.29	0.65
617	265012	948023	-16.22	0.67	-4.47	0.03	-27.97	0.67
618	315012	948023	-16.28	0.66	-4.54	0.03	-28.01	0.66
619	365012	948023	-15	0.67	-4.5	0.03	-25.5	0.67
620	415012	948023	-14.88	0.67	-4.34	0.04	-25.41	0.67
621	465012	948023	-15.12	0.61	-4.26	0.04	-25.99	0.61
622	515012	948023	-15.04	0.64	-4.23	0.04	-25.86	0.64
648	215012	898023	-16.52	0.66	-4.37	0.04	-28.67	0.66
649	265012	898023	-16.06	0.64	-4.55	0.03	-27.58	0.64
650	315012	898023	-15.89	0.64	-4.55	0.03	-27.23	0.64
651	365012	898023	-14.95	0.64	-4.49	0.03	-25.41	0.64
652	415012	898023	-14.52	0.65	-4.41	0.04	-24.63	0.65
653	465012	898023	-14.78	0.63	-4.25	0.03	-25.3	0.63
654	515012	898023	-14.62	0.55	-4.28	0.04	-24.96	0.55
681	265012	848023	-16.41	0.68	-4.53	0.03	-28.29	0.68
682	315012	848023	-16.11	0.67	-4.4	0.03	-27.82	0.67
683	365012	848023	-15.22	0.64	-4.43	0.03	-26.01	0.64
684	415012	848023	-14.86	0.69	-4.32	0.03	-25.4	0.69
685	465012	848023	-15.06	0.64	-4.18	0.03	-25.94	0.64
686	515012	848023	-14.96	0.59	-4.2	0.03	-25.73	0.59
714	315012	798023	-16.37	0.5	-4.23	0.03	-28.5	0.5
715	365012	798023	-16.08	0.61	-4.24	0.03	-27.91	0.61
716	415012	798023	-15.76	0.68	-4.11	0.03	-27.42	0.68
717	465012	798023	-15.46	0.64	-3.94	0.02	-26.98	0.64

Appendix A continued.

Window	Location (Yukon Albers NAD83)		Centroid depth	Centroid depth	Top depth	Top depth	Base depth	Base depth
	Easting (m)	Northing (m)	Z_o (km)	error (km)	Z_t (km)	error (km)	Z_b (km)	error (km)
718	515012	798023	-15.19	0.65	-4.05	0.03	-26.33	0.65
719	565012	798023	-15.02	0.62	-4.06	0.03	-25.98	0.62
746	315012	748023	-16.39	0.4	-4.3	0.03	-28.48	0.4
747	365012	748023	-15.68	0.51	-4.34	0.03	-27.03	0.51
748	415012	748023	-15.68	0.56	-4.26	0.03	-27.09	0.56
749	465012	748023	-15.48	0.53	-4.11	0.02	-26.85	0.53
750	515012	748023	-15.37	0.62	-4.2	0.03	-26.54	0.62
751	565012	748023	-15.84	0.65	-4.11	0.02	-27.58	0.65
752	615012	748023	-16.09	0.66	-4.11	0.02	-28.07	0.66
782	515012	698023	-15.64	0.62	-4.19	0.03	-27.1	0.62
783	565012	698023	-16.36	0.65	-4.1	0.02	-28.62	0.65
784	615012	698023	-16.81	0.74	-4.02	0.02	-29.6	0.74
814	515012	648023	-15.57	0.6	-3.83	0.03	-27.31	0.6
815	565012	648023	-16.66	0.58	-4.02	0.03	-29.31	0.58
816	615012	648023	-16.76	0.61	-3.97	0.02	-29.54	0.61
817	665012	648023	-17.54	0.83	-4.25	0.04	-30.83	0.83
824	1015012	648023	-23.47	1.19	-11.42	0.24	-35.53	1.21
846	515012	598023	-16.48	0.71	-3.53	0.03	-29.42	0.71
847	565012	598023	-17.89	0.76	-3.37	0.03	-32.41	0.77
848	615012	598023	-17.51	0.73	-3.57	0.03	-31.45	0.73
849	665012	598023	-17.83	0.88	-3.5	0.04	-32.16	0.88
850	715012	598023	-17.1	0.82	-3.45	0.05	-30.74	0.83
851	765012	598023	-19.18	0.97	-4.38	0.06	-33.97	0.97
852	815012	598023	-20.3	1.01	-5	0.06	-35.6	1.01
853	865012	598023	-21.54	1.01	-5.46	0.11	-37.62	1.02
854	915012	598023	-21.83	1.09	-5.29	0.09	-38.37	1.1
855	965012	598023	-23.34	1.21	-9.67	0.06	-37.01	1.21
856	1015012	598023	-24.14	1.28	-11.06	0.2	-37.22	1.3
881	665012	548023	-17.63	0.59	-3.51	0.05	-31.76	0.59
882	715012	548023	-17.71	0.52	-3.37	0.07	-32.05	0.52
883	765012	548023	-18.34	0.59	-7.22	0.11	-29.47	0.6
884	815012	548023	-20.06	1.18	-7.98	0.04	-32.15	1.18
885	865012	548023	-21.88	1.02	-10.64	0.17	-33.11	1.04
886	915012	548023	-22.12	1.13	-10.59	0.14	-33.65	1.14
887	965012	548023	-24.23	1.36	-10.28	0.11	-38.18	1.37
888	1015012	548023	-23.22	1.17	-11.08	0.17	-35.35	1.19

Appendix B. List of Zo, Zt, and Zb values, Tanaka method 300 km windows

Window	Location (Yukon Albers NAD83)		Centroid depth	Centroid depth	Top depth	Top depth	Base depth	Base depth
	Easting (m)	Northing (m)	Z_o (km)	error (km)	Z_t (km)	error (km)	Z_b (km)	error (km)
79	103521	1356200	-19.88	0.86	-4.78	0.05	-34.98	0.86
80	153532	1356200	-21.39	0.91	-4.76	0.06	-38.02	0.92
81	203543	1356200	-21.24	1.19	-4.94	0.08	-37.53	1.2
94	103521	1306189	-20.75	0.63	-4.29	0.07	-37.21	0.63
95	153532	1306189	-21.48	0.72	-4.26	0.07	-38.71	0.72
96	203543	1306189	-21.86	0.79	-4.25	0.08	-39.48	0.8
109	103521	1256178	-19.66	0.65	-1.74	0.02	-37.59	0.65
110	153532	1256178	-20.54	0.73	-1.9	0.02	-39.17	0.73
111	203543	1256178	-20.7	0.78	-1.82	0.02	-39.58	0.78
112	253555	1256178	-21.15	1.09	-2.15	0.04	-40.15	1.09
124	103521	1206166	-18.25	0.63	-1.64	0.02	-34.86	0.63
125	153532	1206166	-19.05	0.71	-1.63	0.02	-36.46	0.71
126	203543	1206166	-19.25	0.78	-1.63	0.02	-36.88	0.78
127	253555	1206166	-19.66	1.01	-1.87	0.02	-37.45	1.01
137	315012	1648023	-27.24	0.98	-2.78	0.05	-51.7	0.98
138	365012	1648023	-25.38	0.91	-2.99	0.04	-47.77	0.91
138	53509	1156255	-18.03	0.63	-1.45	0.01	-34.61	0.63
139	103521	1156255	-18.11	0.65	-1.51	0.01	-34.71	0.65
140	153532	1156255	-18.66	0.71	-1.47	0.01	-35.86	0.71
141	203543	1156255	-19	0.76	-1.41	0.01	-36.59	0.76
142	253555	1156255	-19.74	0.97	-1.67	0.02	-37.82	0.97
153	53509	1106244	-16.9	0.58	-1.41	0.02	-32.39	0.58
154	103521	1106244	-16.58	0.62	-1.45	0.02	-31.72	0.62
155	153532	1106244	-16.68	0.66	-1.44	0.02	-31.93	0.66
156	203543	1106244	-16.37	0.66	-1.42	0.02	-31.31	0.66
157	253555	1106244	-16.68	0.84	-1.5	0.02	-31.86	0.84
168	53509	1056233	-16.8	0.53	-1.59	0.02	-32.01	0.53
169	315012	1598023	-26.91	0.91	-2.91	0.08	-50.92	0.92
169	103521	1056233	-16.34	0.54	-1.6	0.02	-31.09	0.54
170	365012	1598023	-24.97	0.83	-3.07	0.06	-46.88	0.83
170	153532	1056233	-16.39	0.58	-1.64	0.02	-31.13	0.58
171	203543	1056233	-16.13	0.56	-1.65	0.02	-30.61	0.56
183	53509	1006221	-17.58	0.58	-1.75	0.02	-33.41	0.58
184	103521	1006221	-17.05	0.61	-1.68	0.02	-32.43	0.61
185	153532	1006221	-16.88	0.65	-1.66	0.02	-32.1	0.65
186	203543	1006221	-16.05	0.61	-1.66	0.02	-30.44	0.61
201	315012	1548023	-26.58	0.84	-3.19	0.08	-49.96	0.84

Appendix B continued.

Window	Location (Yukon Albers NAD83)		Centroid depth	Centroid depth	Top depth	Top depth	Base depth	Base depth
	Easting (m)	Northing (m)	Z_o (km)	error (km)	Z_t (km)	error (km)	Z_b (km)	error (km)
202	365012	1548023	-25.01	0.87	-3.19	0.08	-46.83	0.87
233	315012	1498023	-25.88	0.96	-3.15	0.11	-48.61	0.96
234	365012	1498023	-25.46	0.98	-3.04	0.08	-47.87	0.98
265	315012	1448023	-25.89	0.99	-3.33	0.13	-48.45	0.99
266	365012	1448023	-25.86	1.03	-3.28	0.13	-48.44	1.04
267	415012	1448023	-26.14	1.04	-3.28	0.13	-49	1.05
297	315012	1398023	-25.91	0.96	-3.3	0.13	-48.53	0.96
298	365012	1398023	-25.53	0.98	-3.2	0.13	-47.85	0.99
299	415012	1398023	-25.7	0.95	-3.23	0.13	-48.18	0.96
328	265012	1348023	-28.35	1.19	-2.85	0.11	-53.84	1.19
329	315012	1348023	-26.38	1.05	-3.35	0.13	-49.42	1.06
360	265012	1298023	-27.04	1.12	-4.1	0.06	-49.98	1.12
361	315012	1298023	-25.57	1	-4.31	0.07	-46.83	1.01
392	265012	1248023	-23.03	1.15	-4.19	0.02	-41.87	1.15
393	315012	1248023	-23.61	0.99	-4.25	0.03	-42.97	0.99
424	265012	1198023	-21.78	1.06	-4.18	0.03	-39.38	1.06
425	315012	1198023	-22.18	1.02	-4.28	0.03	-40.08	1.02
426	365012	1198023	-22.27	1.07	-4.46	0.03	-40.07	1.07
456	265012	1148023	-21.34	0.97	-4.11	0.02	-38.58	0.97
457	315012	1148023	-21.59	0.99	-4.21	0.02	-38.97	0.99
458	365012	1148023	-21.44	0.99	-4.43	0.03	-38.45	0.99
488	265012	1098023	-18.7	0.84	-4.15	0.03	-33.26	0.84
489	315012	1098023	-19.17	0.86	-4.4	0.03	-33.95	0.86
490	365012	1098023	-18.96	0.86	-4.63	0.04	-33.29	0.86
520	265012	1048023	-18.04	0.67	-4.22	0.03	-31.86	0.67
521	315012	1048023	-18.71	0.77	-4.36	0.02	-33.06	0.77
522	365012	1048023	-18.72	0.75	-4.39	0.04	-33.05	0.75
551	215012	998023	-16.79	0.59	-4.26	0.03	-29.31	0.59
552	265012	998023	-16.84	0.57	-4.29	0.03	-29.38	0.57
553	315012	998023	-16.7	0.58	-4.41	0.03	-28.99	0.58
554	365012	998023	-16.47	0.55	-4.42	0.03	-28.53	0.55
555	415012	998023	-16.09	0.61	-4.37	0.04	-27.81	0.61
583	215012	948023	-16.73	0.53	-4.26	0.03	-29.21	0.53
584	265012	948023	-16.31	0.54	-4.34	0.03	-28.29	0.54
585	315012	948023	-16.25	0.56	-4.43	0.03	-28.07	0.56
586	365012	948023	-16.07	0.54	-4.47	0.03	-27.66	0.54
587	415012	948023	-15.44	0.53	-4.42	0.02	-26.46	0.53
588	465012	948023	-15.8	0.48	-4.22	0.05	-27.39	0.48

Appendix B continued.

Window	Location (Yukon Albers NAD83)		Centroid depth	Centroid depth	Top depth	Top depth	Base depth	Base depth
	Easting (m)	Northing (m)	Z_o (km)	error (km)	Z_t (km)	error (km)	Z_b (km)	error (km)
617	315012	898023	-16.15	0.53	-4.42	0.03	-27.87	0.53
618	365012	898023	-15.99	0.52	-4.45	0.03	-27.53	0.52
619	415012	898023	-15.49	0.52	-4.39	0.02	-26.59	0.52
620	465012	898023	-15.25	0.51	-4.28	0.03	-26.23	0.51
649	315012	848023	-16.61	0.4	-4.35	0.03	-28.87	0.4
650	365012	848023	-16.52	0.43	-4.31	0.03	-28.72	0.43
651	415012	848023	-16.05	0.51	-4.2	0.02	-27.91	0.51
652	465012	848023	-15.74	0.52	-4.09	0.02	-27.39	0.52
681	315012	798023	-16.48	0.37	-4.37	0.02	-28.6	0.37
682	365012	798023	-16.47	0.4	-4.34	0.02	-28.6	0.4
683	415012	798023	-15.83	0.46	-4.31	0.02	-27.36	0.46
684	465012	798023	-15.7	0.47	-4.24	0.02	-27.16	0.47
685	515012	798023	-15.99	0.46	-4.08	0.03	-27.89	0.46
717	515012	748023	-15.86	0.44	-4.17	0.02	-27.56	0.44
750	565012	698023	-16.14	0.52	-3.93	0.03	-28.35	0.52
751	615012	698023	-16.95	0.48	-4.03	0.02	-29.88	0.49
782	565012	648023	-16.85	0.58	-3.6	0.03	-30.11	0.58
783	615012	648023	-17.78	0.63	-3.56	0.02	-32.01	0.63
816	665012	598023	-18.49	0.52	-3.75	0.03	-33.23	0.52
817	715012	598023	-18.35	0.54	-3.73	0.04	-32.97	0.54
818	765012	598023	-18.34	0.57	-3.69	0.04	-33	0.57
819	815012	598023	-20.25	0.71	-3.75	0.06	-36.76	0.71
820	865012	598023	-21.62	0.95	-4.61	0.05	-38.64	0.95
821	915012	598023	-23.58	1.06	-4.93	0.06	-42.23	1.06
822	965012	598023	-24.72	0.97	-4.79	0.05	-44.65	0.97
848	665012	548023	-17.93	0.45	-3.94	0.04	-31.92	0.46
849	715012	548023	-17.61	0.48	-3.94	0.06	-31.28	0.48
850	765012	548023	-17.61	0.52	-4.03	0.06	-31.2	0.53
851	815012	548023	-18.21	0.65	-4.7	0.08	-31.71	0.65
852	865012	548023	-18.19	0.8	-4.92	0.11	-31.45	0.81
853	915012	548023	-21.48	0.96	-5.34	0.11	-37.62	0.97
854	965012	548023	-24.15	0.95	-4.05	0.06	-44.26	0.95
855	1015012	548023	-26.87	1	-3.5	0.11	-50.23	1.01

Appendix C. CPD map using Bansal method and 200 km window.

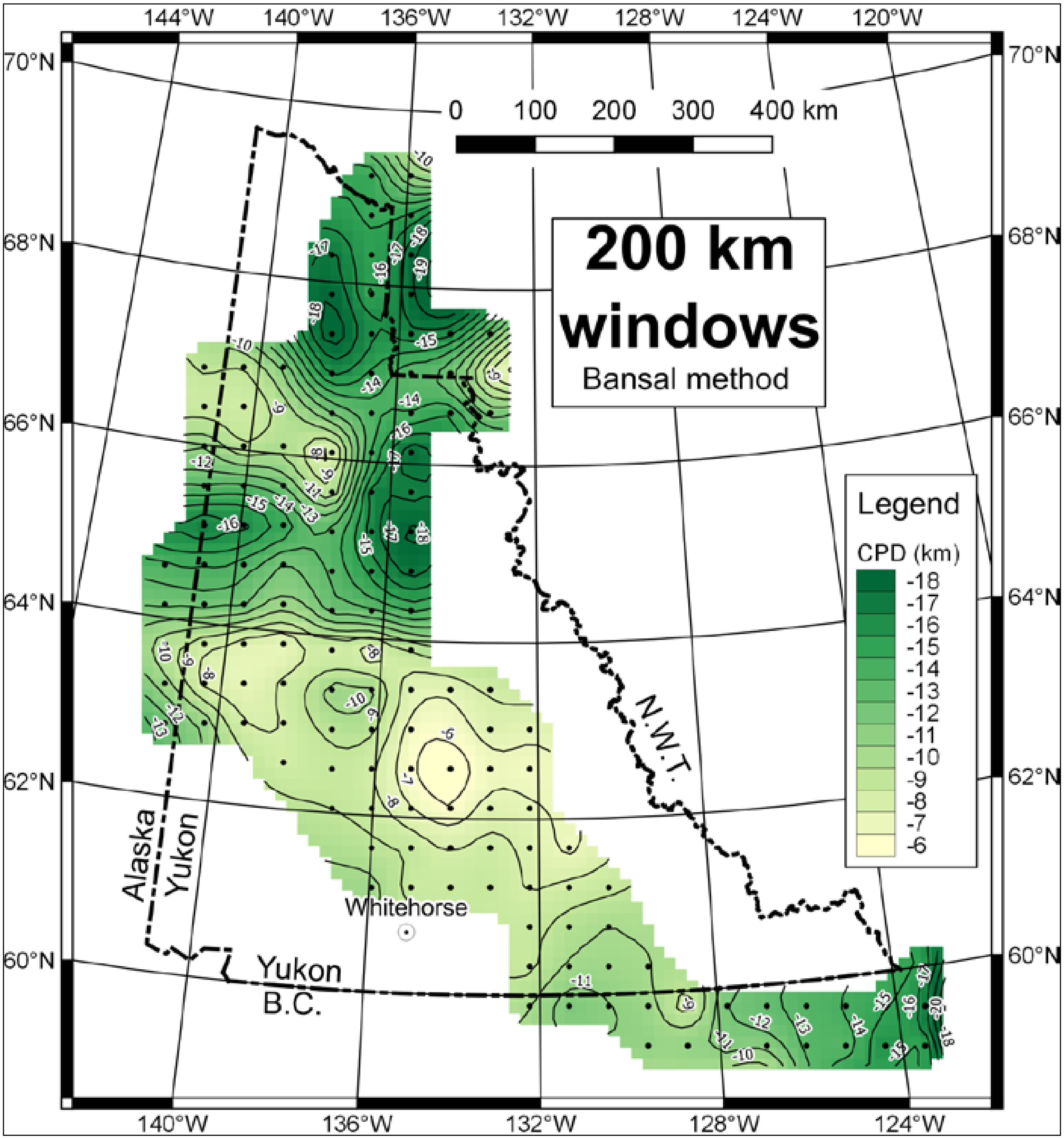

Figure C1. *Curie point depth map for Yukon using 200 km windows and the Bansal et al. (2011) method (fractal magnetic sources, β=2). The window centres are shown as black dots. Yellow and green colours represent shallow and deep CPD estimates, respectively. Contour lines show CPD in units of kilometres below the surface. Our interpretation is that these results are not an accurate representation of the depth to the Curie point in Yukon due to limitations of the method discussed in the text. They are included here simply as an illustration of the results using the Bansal method.*

Appendix D. CPD map using Bansal method and 300 km windows

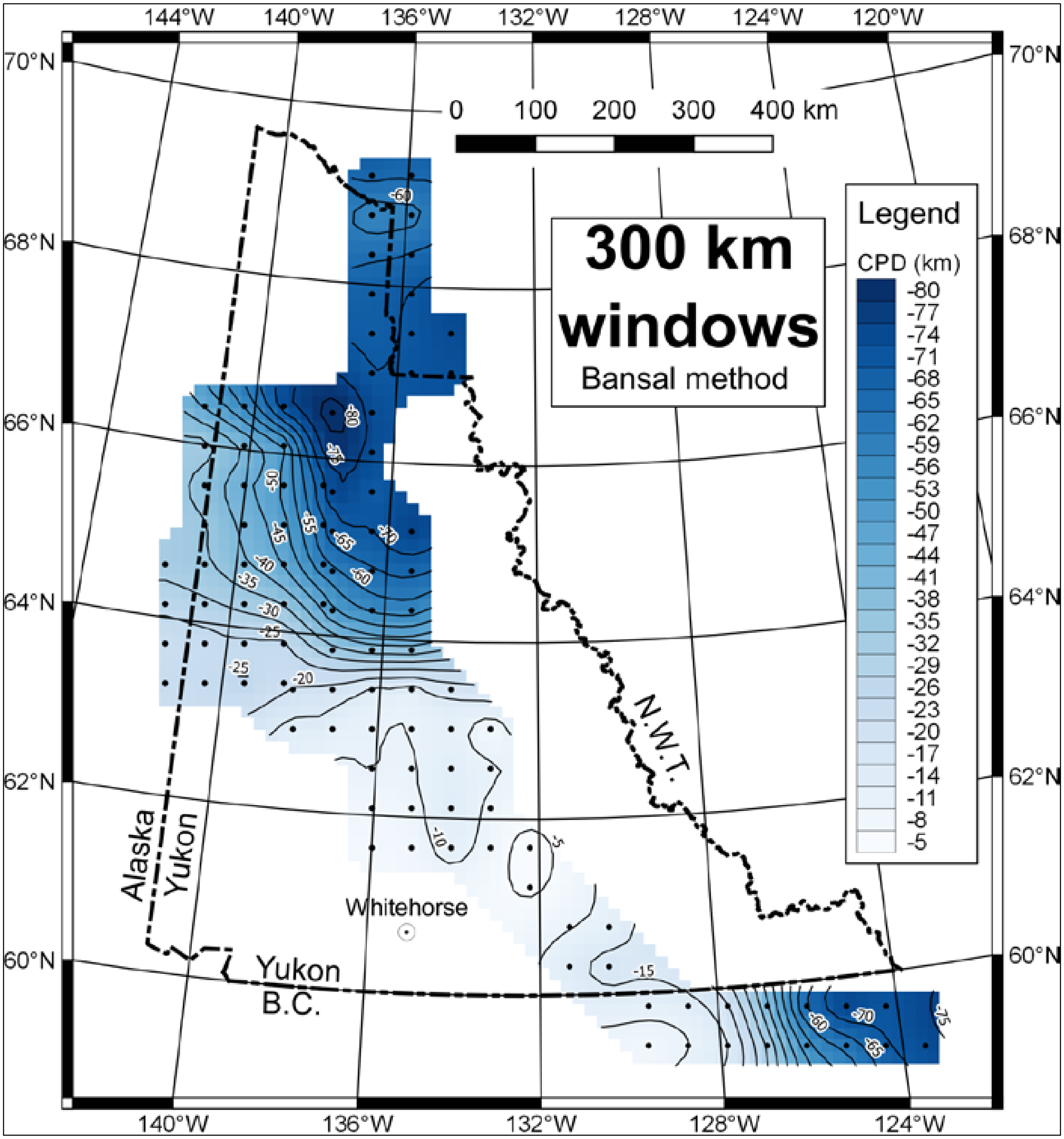

Figure D1. *Curie point depth map for Yukon using 300 km windows and the Bansal et al. (2011) method (fractal magnetic sources, β=2). The window centres are shown as black dots. White and blue colours represent shallow and deep CPD estimates, respectively. Contour lines show CPD in units of kilometres below the surface. Our interpretation is that these results are not an accurate representation of the depth to the Curie point in Yukon due to limitations of the method discussed in the text. They are included here simply as an illustration of the results using the Bansal method.*

Appendix E. Statement of Qualifications

This report has been prepared by Jeffrey B. Witter, Principal Geoscientist at Innovate Geothermal Ltd. Dr. Witter holds an undergraduate degree in geophysics as well as Master's and PhD degrees in geology. He has eleven years of experience as an exploration geologist/geophysicist in the natural resource industry with about half of that time committed specifically to geothermal exploration and resource evaluation. He is a registered professional geoscientist in the province of British Columbia (Canada) and is a member of the Association of Professional Engineers and Geoscientists of British Columbia (APEGBC). APEGBC has a defined and enforceable Code of Ethics which Dr. Witter agrees to abide by. Dr. Witter has been engaged as a Consultant by the Yukon Geological Survey.

Dated in Vancouver, British Columbia, Canada this 31st day of March 2017

Jeffrey B. Witter Ph.D., PGeo (Province of British Columbia, No. 36004)